CRUSTAL STRUCTURE AND GEOLOGIC HISTORY OF THE ESPINO RIFT, VENEZUELA, BASED ON INTEGRATION OF POTENTIAL FIELDS, SEISMIC REFLECTION, AND WELL DATA

A Thesis Presented to

the Faculty of the Department of Earth and Atmospheric Sciences

University of
Houston

In Partial Fulfillment

of the Requirements for the Degree

Master of Science

By

Lourdes Gabriela Del Carmen Rodríguez Milano

August 2016

CRUSTAL STRUCTURE AND GEOLOGIC HISTORY OF THE ESPINO RIFT, VENEZUELA, BASED ON INTEGRATION OF POTENTIAL FIELDS, SEISMIC REFLECTION, AND WELL DATA

Lourdes Gabriela Del Carmen Rodríguez Milano

APPROVED:

Dr. Paul Mann, Chairman

Dr. Stuart Hall

Peter Bartok, Bartok Incorporated

Dr. Dan Wells, Dean
College of Natural Sciences and Mathematics

Dedication

To my parents, Elinor and Euclides,
thank you for everything.

ACKNOWLEDGEMENTS

I would like to thank my research advisor, Dr. Paul Mann, for letting me become part of the Caribbean Basins, Tectonics, and Hydrocarbons (CBTH) team and for his continuous support during my master studies. Special thanks go to Dr. Stuart Hall. Thank you for the patience, encouragement, support, and time. Thank you for showing me the other side of geophysics I never had the chance to work with before, potential, and thank you for making it interesting and exciting. In the non-unique world of potential fields you are a unique, and excellent, professor. I would like to thank Peter Bartok from Bartok Incorporated for accepting to be part of my committee and for sharing his extensive knowledge in the geology of Venezuela with me during this project. Thanks to PDVSA Exploración and Ing. José Benavides for providing the seismic reflection data. I would like to acknowledge Luan Nguyen, Naila Dowla, and Shenelle Gomez for their constant help with gravity and magnetic analysis; and Javier Sánchez for his help in seismic interpretation. I would like to thank my friends and colleagues Fabiola Ruíz, Mari Tesi, Joan Marie Blanco, Naila Dowla, Shenelle Gomez, Lucia Torrado, and Lily Schaffer for your support and for making these two years fun and exciting. Thanks to all the CBTH team for their assistance.

Thanks to my family for their support and love, specially my parents Elinor and Euclides. Thank you for listening to me, for your support throughout all these years and for making me believe in myself in the most difficult moments. I love you with all my heart. Thanks to my soul mate, Abdullrahman, for giving me the strength and support I needed, I love you. Finally, thanks to Simba for bringing me joy with his four paws.

CRUSTAL STRUCTURE AND GEOLOGIC HISTORY OF THE ESPINO RIFT, VENEZUELA, BASED ON INTEGRATION OF POTENTIAL FIELDS, SEISMIC REFLECTION, AND WELL DATA

An Abstract of a Thesis

Presented to

the Faculty of the Department of Earth and Atmospheric Sciences

University of Houston

In Partial Fulfillment

of the Requirements for the Degree

Master of Science

By

Lourdes Gabriela del Carmen Rodríguez Milano

August 2016

ABSTRACT

The Espino rift of north-central Venezuela is a 60-100-km-wide, 250-km-long symmetrical, subsurface rift that formed in Cambrian-Ordovician time and experienced a second phase of rifting during the late Jurassic breakup of Pangea. During Oligocene and Miocene, normal faults bounding the Espino rift were reactivated especially at its northern end by transpression between the eastward-moving Caribbean plate and the northern margin of South America. During this period, the Espino rift became deeply buried beneath the Eastern Venezuela foreland basin. I apply filters to gravity and magnetic data from the region of the Espino rift in central Venezuela to delineate the crustal setting of the rift I use three 2D gravity transects combined with five seismic reflection transects tied to twelve wells to reconstruct the multi-stage geologic and structural evolution of the Espino rift from its initial rift phase in Cambrian-Ordovician time through its subsequent period of rifting during the latest Jurassic, and a final period of Oligocene-Miocene tectonic transpression related to the oblique collision of the Great Arc of the Caribbean with northern South America. Because there is no direct well evidence for the type and age of basement underlying the Espino rift, my gravity and magnetic transects provide new observations on crustal thickness variations across and along the rift which ranges from 13 to 30 km. Gravity modeling also reveals a variation in Moho depths from ~30 km on its rift flanks to 24-29 km beneath the rift axis. These data constrain the subsurface extent of the rift that can be traced for 200 km along-strike from a shallow rift in the south (basement 1.8 km beneath the rift axis) to a central rift area (basement 12 km beneath the rift axis) to a zone of Cenozoic tectonic transpression in the northern rift area (basement 10 km beneath

the rift axis). Based on wells and seismic reflection data, I infer that the Cambro-Ordovician rift phase was accompanied by a greater degree of crustal thinning than the late Jurassic rift phase.

TABLE OF CONTENTS

Figure captions

CHAPTER 1: INTRODUCTION TO THIS THESIS

1.1 DEVELOPMENT OF THIS THESIS

After completing my BS degree in Geophysical Engineering in May, 2014, from Simón Bolívar University in Caracas, Venezuela, I began the master in geophysics at the Department of Earth and Atmospheric Sciences of the University of Houston in August 2014 to work with Dr. Paul Mann and the Caribbean Basins, Tectonics, and Hydrocarbons (CBTH). For my master's research, I obtained seismic reflection and well data from the area of the Espino rift of north-central Venezuela that was kindly provided by Ing. Benavides of Petróleos de Venezuela S.A. (PDVSA) for my master's research study.

The goal of my master's study was to gain a better understanding of the multi-phase, geologic and tectonic history of the Espino rift and its surrounding crustal provinces (Fig. 2A) by combining the seismic reflection data provided to me by PDVSA with filtered and enhanced maps of regional gravity and magnetic data that were obtained both from publicly available, online datasets and from Dr. Crelia Padrón at Simon Bolivar University in Caracas, Venezuela. The PDVSA seismic reflection data had been previously partially interpreted by Salazar (2006) as part of her bachelor's thesis study at the Universidad Central in Caracas, Venezuela. I hoped to expand on the previous study by Salazar (2006), which focused on the shallower, sedimentary section. The goal of my thesis was to integrate gravity and magnetic data to better understand the deeper crustal structure of the rift and to compare these results to previous gravity studies of deeper crustal structure by

Schmitz et al. (2008) and to integrate the links between the deeper, crustal structure of the rift and its overlying sedimentary units.

In addition to Dr. Mann who had worked primarily on Cenozoic rocks in Venezuela (Escalona and Mann, 2011), my University of Houston master's committee included Mr. Peter Bartok, adjunct professor at the University of Houston who has an extensive background in the Precambrian and Paleozoic geology of Venezuela (Bartok, 1990), and Dr. Stuart Hall, a professor at the University of Houston, who specializes in the processing and interpretation of regional gravity and magnetic data.

I was also assisted by Andrew Steier, a UH undergraduate student supported by the CBTH project, , who developed the plate model for the area of the Espino rift (Fig. 1), and Nawaz Bugti, a researcher with the CBTH project, who assisted me with the construction of burial plot for the Espino rift.

During my two-year master's study, I took graduate level courses at the University of Houston that included: structure, stratigraphy, 3D interpretation of seismic reflection data, potential fields data analysis, and geology of the Caribbean and northern South America. I was also a member the five-person University of Houston Imperial Barrel Award (IBA) team that competed in the AAPG Gulf Coast competition during the spring semester of 2015. In addition to research and classes at the University of Houston I began working part-time for Sanchez Oil & Gas in Houston as a geophysicist and will continue that job as a fulltime employee following completion of my master's degree in August, 2016.

1.2 SUMMARY OF PREVIOUS STUDIES MOST RELEVANT TO MY MASTER'S PROJECT

The EVB along with the underlying Espino rift have been studied intensively for several decades because the EVB is the second most productive, hydrocarbon basin in Venezuela. The Espino rift is a deep rift (2-12 km sedimentary thickness) and for this reason the depth to the top basement surface is difficult to identify using seismic reflection and well data alone. Garcia (2009) conducted a regional, gravity analysis of northern Venezuela that included the area of the Espino rift. Her gravity map - based on contoured gravity readings observed from gravity stations across the rift - shows a sedimentary response to the northeast, which was inferred to represent the deepest part of the Espino rift. Thicker, syn-rift fill in the central and northeastern part of the rift was consistent with the idea that the rift formed along the same axis during two distinct, rift periods: one in the early Paleozoic, and the second during the late Jurassic. The gravity response of the area was complicated by the presence of the thick sedimentary fill of the EVB deposited above the Espino rift during the oblique collision of the Caribbean plate with northern South America (Jácome et al., 2008).

Salazar (2006) used a grid of seismic data provided by PDVSA to map unconformities, which she used to subdivide the rift stratigraphy into different periods of tectonic activity. Her mapping of the seismic grid tied to wells also delineated major geological features of the rift (e.g. bounding faults, depocenters). Salazar (2006) also made a structural restoration of the Espino rift based on deep seismic refraction studies done by Schmitz et al. (2002).

Ríos (2002) generated gravity and magnetic models along two, regional gravity transects to estimate the Jurassic, syn-rift sedimentary thickness in the Espino rift. The modeled thickness of syn-rift, sedimentary rocks showed a thicker section in the central and northeastern parts of the rift. Gravity models of basalt flows known from deep wells showed that their distribution is entirely contained by the limits of the Espino rift.

CHAPTER 2: CRUSTAL STRUCTURE AND GEOLOGIC HISTORY OF THE ESPINO RIFT, VENEZUELA, BASED ON INTEGRATION OF POTENTIAL FIELDS, SEISMIC REFLECTION, AND WELL DATA.

2.1 INTRODUCTION

2.2.1 Significance of the Espino rift of Venezuela

The Espino rift is a result of the Cambrian rifting, which occurred after the Precambrian orogenic events in northern South America (Bellizzia, 1972; Bartok, 1993) and during the deposition of mainly marine shale of the Cambro-Ordovician Carrizal and Hato Viejo formations (Fig. 1). Paleozoic reconstructions of northern South America support the late Paleozoic (Ordovician-Permian) as key periods of deformation related to the collision of Gondwana with the Laurasian plate. This collision is related to the Caledonian Orogeny, which was caused by the closure of the Iapetus Ocean generating a suture zone across plates (purple line shown in Fig. 1). (Dalla Salda, et al., 1992; Kroner and Stern, 2004; Bartok, 1993). The reactivation of the Cambrian rift occurred in the Jurassic as South America rifted from North American during the opening of the central Atlantic generating the proto-Caribbean sea. Finally, the late Cretaceous-present collision of the Caribbean plate with the northern South American plate generated the Eastern Venezuelan foreland basin, which overlies the Espino rift.

The 175-km long Espino rift of north-central Venezuela in northern South America overlies a late Paleozoic, northeast-striking, crustal suture zone separating the Paleozoic orogenic belt to the northwest from the Precambrian Guayana shield to the southeast (Fig. 1). My subsurface study area of the Espino rift is located beneath the Guárico sub-basin to the western part of the Eastern Venezuela foreland basin (EVB) (Fig. 2A). The asymmetrical EVB overlies and depresses northward-dipping, igneous-metamorphic basement of Precambrian age and a Cretaceous to Oligocene passive margin (Hedberg, 1960; Escalona and Mann, 2011).

As the Espino rift is deeply buried beneath Cenozoic rocks of the EVB and Cretaceous rocks of the passive margin, rocks of the Espino rift do not outcrop and are only known from potential field studies, seismic reflection surveys, and a few, widely-spaced, exploration wells in the area. Previous, seismic reflection studies tied to wells have shown that the earlier Cambrian rift was reactivated by the late Jurassic rifting event associated with the separation of North and South America (Bartok, 1993; Salazar, 2006).

Figure 2A summarizes in map view the Phanerozoic plate tectonic history of the Espino rift, which includes several phases of tectonic activity extending form the Cambrian to the present-day:

1) Cambrian rifting (Bartok, 1993; Pelechaty, 1996)
2) Late Paleozoic collision (Williams, 1995; Ross and Scotese, 1988; Speed et al., 1997; Moreno-López and Escalona, 2014);
3) Jurassic rifting (Parnaud et al., 1995);
4) Late Cretaceous to present oblique collision with foreland basin formation (Escalona and Mann, 2011).

Figure 1. Precambrian to present-day plate reconstructions of the Espino rift in northern South America (boxed area) showing the tectonic evolution of the Espino rift area through time (plate reconstructions are modified from Seton et al. (2012). and were prepared by UH undergraduate student Andrew Steier in 2016). Distribution of rifts and their ages identified by the color code in the key is from Sengor and Natal'in (2001). Purple line shows Caledonian suture (modified from Restrepo-Pace et al., 1997; Kröner and Stern, 2005 and Dalla Salda et al., 1992) A) In Early Cambrian, the Espino rift forms during opening of Paleotethys and Iapetus Oceans; B) In Permian, continental collision occurs between North and South America during the assembly of the Pangean supercontinent and the Paleozoic orogenic belt is sutured onto the Guayana Precambrian shield in the area of the Espino rift; C) In late Jurassic, the breakup of the Pangean supercontinent leads to a second phase of extension accompanied by volcanism in the Espino rift; D) In late Cretaceous, passive margin subsidence affects the Espino rift and northern margin of South America; E) in early Miocene, oblique collision between the Great Arc of the Caribbean and northern South America creates the Eastern Venezuelan foreland basin that deeply buries the northern end of the Espino rift; and F) in the present-day, the Espino rift continues to be buried beneath continental and fluvial sedimentation in the Eastern Venezuelan foreland basin and Orinoco River valley.

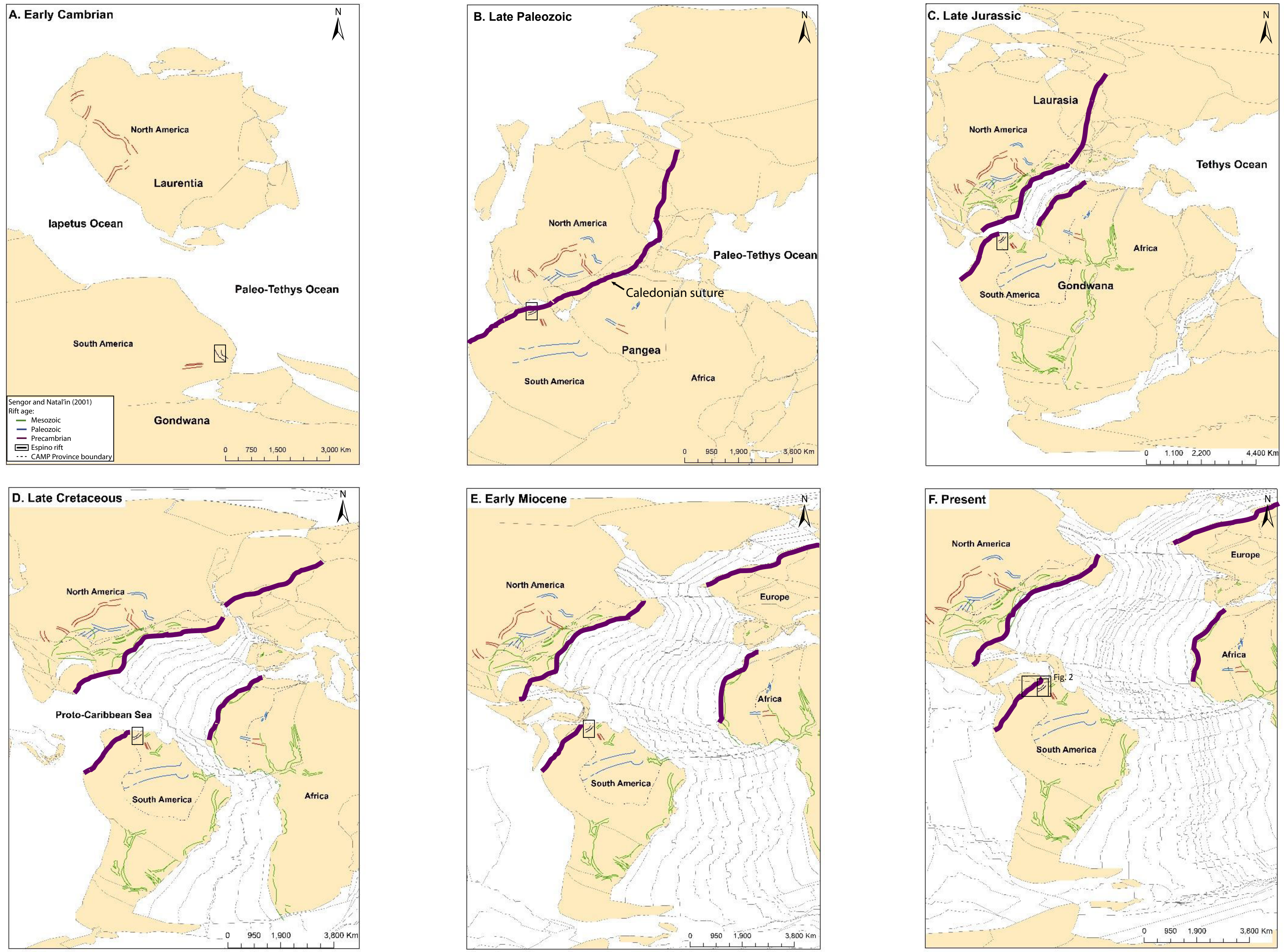
A. Early Cambrian
North America
Laurentia
Iapetus Ocean
Paleo-Tethys Ocean
South America
Gondwana
Sengor and Natal'in (2001)
Rift age:
Mesozoic
Paleozoic
Precambrian
Espino rift
CAMP Province boundary
0 750 1,500 3,000 Km
B. Late Paleozoic
North America
Paleo-Tethys Ocean
Caledonian suture
Pangea
South America
Africa
0 950 1,900 3,800 Km
C. Late Jurassic
Laurasia
North America
Tethys Ocean
Africa
Gondwana
South America
0 1,100 2,200 4,400 Km
D. Late Cretaceous
North America
Proto-Caribbean Sea
South America
Africa
0 950 1,900 3,800 Km
E. Early Miocene
North America
Europe
Africa
South America
0 950 1,900 3,800 Km
F. Present
North America
Europe
Africa
Fig. 2
South America
0 950 1,900 3,800 Km

The Cenozoic foreland basin section of the EVB overlying the Espino rift has been widely studied for many decades for its oil potential based on mature, Cretaceous source rocks of the passive margin overlain by prolific, sandstone reservoirs of the EVB (Audemard and Serrano, 2001). However, there is little known about the Precambrian basement which underlies the Paleozoic though Jurassic, syn-rift sedimentary sections deposited during both phases of rifting. Recent imaging in the Jurassic section of the Espino rift has raised new questions about its deeper sections - such as the Jurassic and the Cambrian-Ordovician Carrizal and Hato Viejo formations - and their petroleum potential (Audemard and Serrano, 2001; Barrios et al., 2011). The Precambrian basement may be a subsurface, northwestern extension of older Precambrian provinces that crop out in the Guayana Shield and have been studied and dated in that area (Ostos et al., 2005).

The global association of giant hydrocarbon reservoirs in continental rift settings has made the Paleozoic-Jurassic, composite Espino rift an important exploration target for hydrocarbons in north-central Venezuela (Audemard and Serrano, 2001). The subsurface Espino rift of Cambrian-Ordovician and late Jurassic age is buried beneath Cenozoic, clastic rocks of the Guárico sub-basin of the Eastern Venezuelan foreland basin in Anzoátegui and Guárico states of north-central Venezuela (Ostos et al., 2005)

The trend of the Espino rift (Fig. 1) is similar to the trend of Cambrian rifts in eastern North America (Bartok, 1993). The Paleozoic Espino rift is similar to the Paleozoic rifts of eastern North America based on their sedimentary fill (red beds, shale and conglomerate) and their lack of metamorphism.

The Central Atlantic magmatic province (CAMP) is a large igneous province mainly composed of basalts in flows and intrusive bodies formed in the Late Triassic-Early Jurassic present in the North and South America, Europe and northwest Africa (Blackburn et al., 2013). The South American extension of this province is relatively close to the Espino rift (Fig. 1). However, the Jurassic basalts found in Well E in the central-north section of the rift are of much younger age (162 Ma) and appear to be an isolated occurrence of igneous activity associated with Late Jurassic crustal thinning of the Espino rift.

2.2 CRUSTAL AND BASINAL SETTING OF THE ESPINO RIFT IN VENEZUELA

2.2.1 Basement crustal provinces of Venezuela

The igneous and metamorphic basement rocks of Venezuela can be divided into three units: a southern Precambrian shield, a transitional Paleozoic belt, and a northern belt of Mesozoic to Tertiary age (Feo-Codecido et al., 1984). The Precambrian terranes crop out in the Guayana Shield as both allochthonous and autochthonous units. (Yoris and Ostos, 1997) (Fig. 2A).

The Guayana Shield is composed of four Precambrian provinces: Imataca, Pastora, Cuchivero, and Roraima (Gonzáles de Juana et al, 1980). The Imataca province is one of the oldest provinces in the Guayana shield (~2700 – 3000 Ma) (Hurley et al., 1973). It is composed mainly of granulites with different mineral composition gneisses along with metamorphosed quartzite and calcite and volcanic intrusions (Fig. 3), and as a second lithology quartzite and calcite heavily metamorphosed with volcanic intrusions (Bellizzia and Martín Bellizzia, 1956). The Pastora province (~2000 Ma) is composed of graywacke, siltstone, and conglomerate slightly metamorphosed with volcanic intrusions and red jasper at its base (Korol, 1965). McCandless (1965) and Briceño et al. (1989) describe the Cuchivero province (~1300 Ma) as extrusive igneous rock (rhyolite) and intrusive igneous rock (granite). Finally, the Roraima province (~1300 – 1500 Ma) is mainly composed of conglomerate, quartz-rich sandstone, and shale interbedded with jasper and volcanic intrusions (Reid, 1974).

Figure 2 A. Surface and subsurface crustal map of Venezuela modified from Ostos et al. (2005) based on a compilation of outcrop, well and potential fields data and showing four crustal types identified in the key. Subsurface faults bounding the Espino rift at depth are modified from Salazar (2006). The oldest crust exposed in the Guayana shield includes four Precambrian provinces characterized by lithologies of different ages: Imataca, Pastora, Cuchivero and Roraima. Lower Paleozoic basins overlying Precambrian or Paleozoic basement were sutured onto the Guayana shield along the approximate trace of the Apure fault and Espino rift during the late Paleozoic assembly of the Pangean supercontinent**. B.** Regional map of Venezuela showing the major, sedimentary basins in light shading along with faults of Cenozoic age. Subsurface faults bounding the Espino rift at depth are modified from Salazar (2006). The study area of the Espino rift is shown in the white box that is keyed to the map shown in Figure 3. Key to abbrevations of faults: EPF = El Pilar fault; APF = Apure fault; ATF = Altamira fault; GTF = Guarico thrust front; UF = Urica fault; and AF = Anaco fault

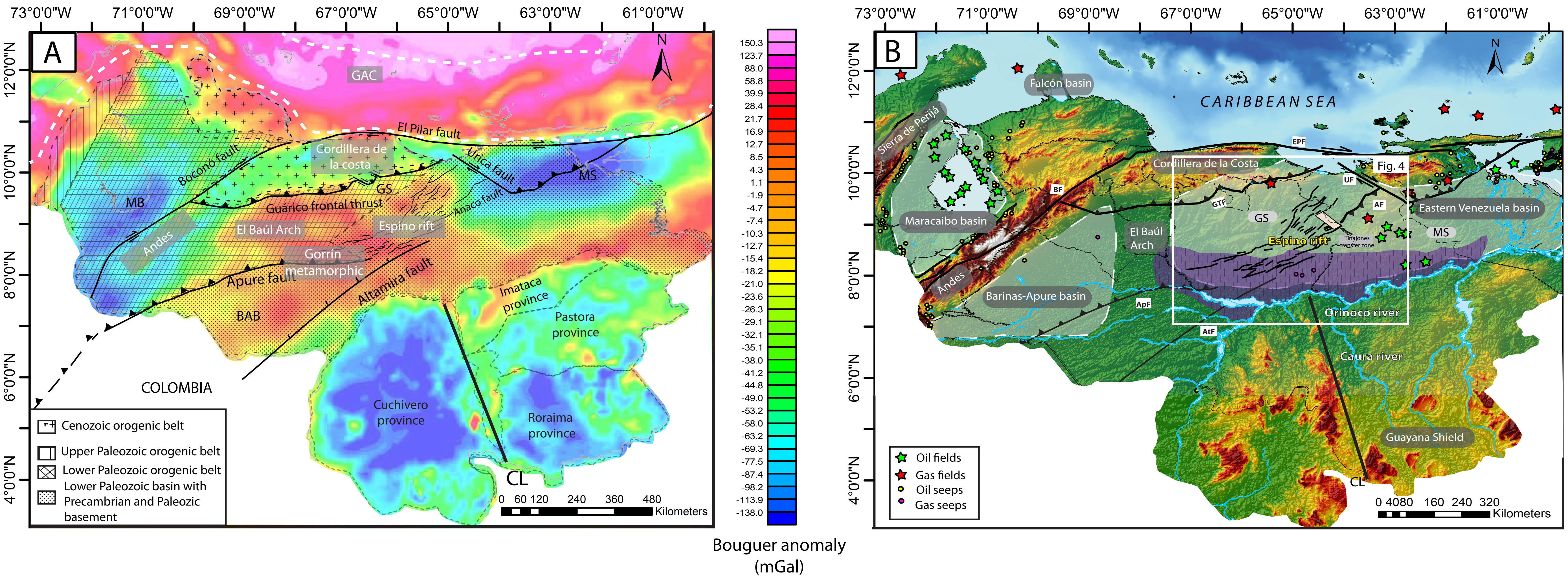

A
B
73°0'0"W
71°0'0"W
69°0'0"W
67°0'0"W
65°0'0"W
63°0'0"W
61°0'0"W
12°0'0"N
10°0'0"N
8°0'0"N
6°0'0"N
4°0'0"N
N
GAC
El Pilar fault
Boconó fault
Cordillera de la costa
Urica fault
Anaco fault
MS
GS
MB
Guárico frontal thrust
El Baúl Arch
Espino rift
Andes
Gorrín metamorphic
Apure fault
Altamira fault
Imataca province
Pastora province
BAB
COLOMBIA
Cuchivero province
Roraima province
CL
Cenozoic orogenic belt
Upper Paleozoic orogenic belt
Lower Paleozoic orogenic belt
Lower Paleozoic basin with Precambrian and Paleozic basement
0 60 120 240 360 480 Kilometers
150.3
123.7
88.0
58.8
39.9
28.4
21.7
16.9
12.7
8.5
4.3
1.1
-1.9
-4.7
-7.4
-10.3
-12.7
-15.4
-18.2
-21.0
-23.6
-26.3
-29.1
-32.1
-35.1
-38.0
-41.2
-44.8
-49.0
-53.2
-58.0
-63.2
-69.3
-77.5
-87.4
-98.2
-113.9
-138.0
Bouguer anomaly (mGal)
Falcón basin
CARIBBEAN SEA
Sierra de Perijá
EPF
Cordillera de la Costa
Fig. 4
UF
BF
GTF
GS
AF
Maracaibo basin
Eastern Venezuela basin
El Baúl Arch
Espino rift
MS
Andes
Barinas-Apure basin
ApF
AtF
Orinoco river
Caura river
Guayana Shield
Oil fields
Gas fields
Oil seeps
Gas seeps
0 4080 160 240 320 Kilometers

During the Late Paleozoic, suturing of Precambrian blocks juxtaposed Precambrian rocks in the north of the Guayana Shield (Bartok, 1993; (Ostos et al., 1997)). The Espino rift is located near the contact or suture zone between the Paleozoic and Precambrian basement (Fig. 2A) (Feo-Codecido et al., 1984). The deepest well in the area was NZZ-88X (called Well E in this study) showing Jurassic basalts interbedded with red beds in the Ipire formation (Fig. 3). The deepest formation this well penetrated was the Carrizal formation of Late Cambrian-Ordovician age and composed of red shale with the presence of Late Cambrian Acrytarchs fossils (Bartok, 1993).

2.2.1 Gravity expression of crustal provinces in Venezuela

The Bouguer anomaly map of the Guayana shield shows negative gravity anomalies between 0 and -140 mGal (Fig. 2A). The most negative values are located in the region of the Cuchivero province and continue with less intensity in the Roraima province to the northeast. The Caura lineament (CL) - which separates Cuchivero from Imataca crustal provinces (Schmitz et al., 2008) - marks the change from negative values of -140 mGal to negatives of ~-30 mGal. The north-northwest orientation of the Caura lineament is also reflected in the parallel trend of the Caura River.

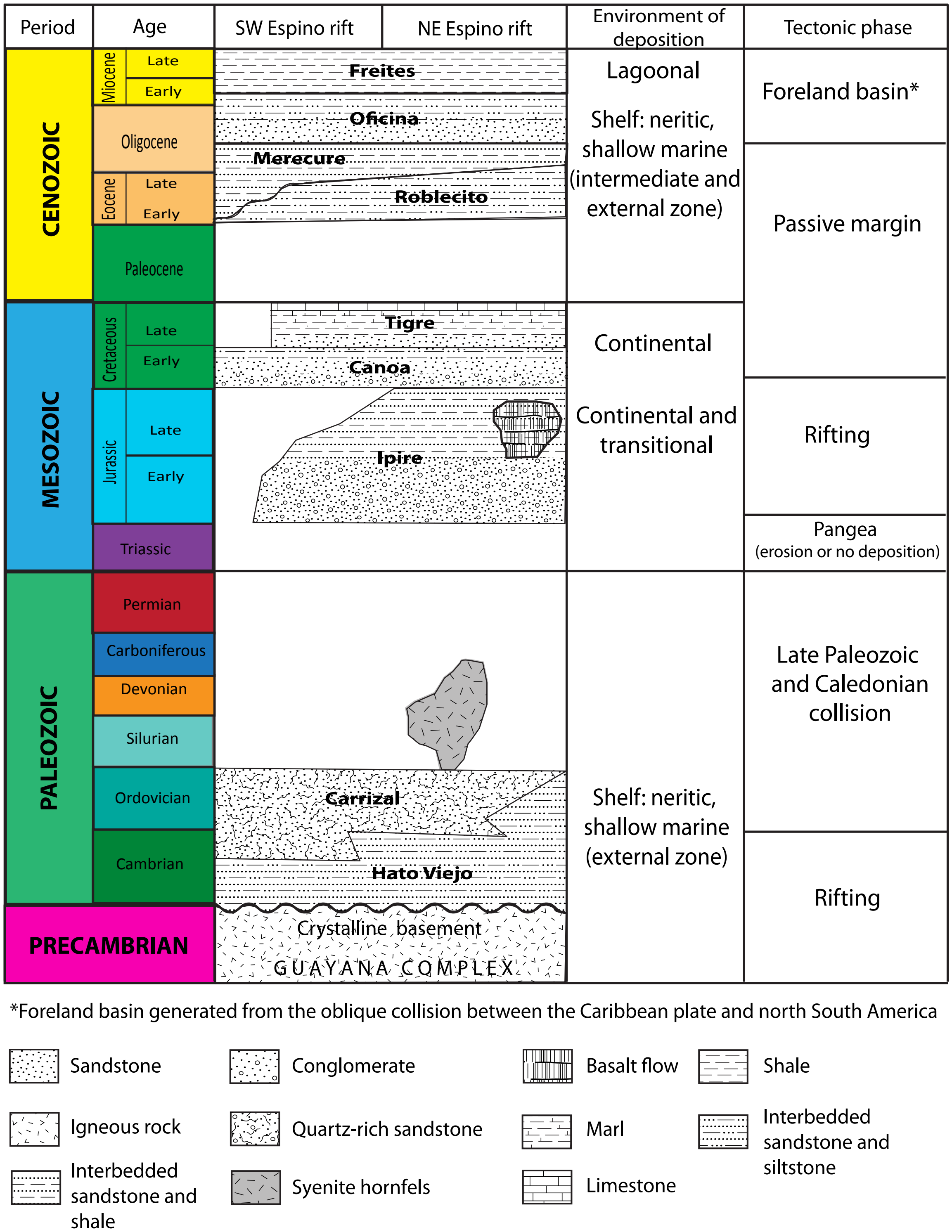

Figure 3. Tectonostratigraphic chart of the Espino rift with columns on the left on the southwestern end of the Espino rift and columns to the right on its northeastern end. Chart is compiled from Galavis and Velarde (1967), Vega and De Rojas (1987), Varela (2004), Salazar (2006) and Durán (2007)

The Imataca province to the northeast, shows gravity values between -10 and -40 mGal, which can be related to differences in mineralogy of rocks present in the area. North of the Guayana shield, the Maturín sub-basin (MS) shows -142 mGal in its depocenter and between -50 and -30 mGal in its surroundings (Fig. 2A).

The Espino rift shows gravitational values between -10 and 15 mGal, which likely reflect the thick, overlying section of the Eastern Venezuelan foreland basin. The Guárico thrust front delimits the Cordillera de la Costa mountain system from the flat-lying sedimentary basin of the Guárico sub-basin and the Barinas-Apure basin (BAB). The southern section of the Great Arc of the Caribbean (GAC) has a prominent, gravity high ranging from 15 mGal to 150 mGal. The active, right-lateral El Pilar fault zone marks the suture zone between the Caribbean plate and northern South America and is expressed by a clear change in the gravitational signal.

2.2.2 Sedimentary basins of Venezuela

The four major Cretaceous-Cenozoic sedimentary basins in Venezuela responsible for almost all of the oil production in the country include: the Maracaibo basin, the Barinas-Apure basin, the Falcón basin and the Eastern Venezuela basin (Fig. 2B).

Maracaibo basin. The Maracaibo basin contains up to 10 km of Cretaceous and Cenozoic sedimentary rocks and covers an area of 52,000 km^2 in the western part of the country (PDV Léxico, 1997). The triangular basin is bounded by several mountain ranges that include the Andes, Sierra de Perijá and Serranía de Trujillo. Miocene and younger uplift of the Andes provided an important structural and burial phase for hydrocarbon accumulations. The main source rock is La Luna formation of Late Cretaceous age, and some of the most important reservoir rocks are Río Negro and Aguardiente formation (Cretaceous) and Lagunillas and La Rosa (Miocene) (Yoris and Ostos, 1997).

Falcon basin. The Falcón basin is located in the northwestern part of Venezuela and is separated from the Maracaibo basin by the Serranía de Trujillo. The Falcon basin formed as the result of tectonic events during the Oligocene and Miocene (Muessig, 1984). A later inversion and folding of the basin fill was generated as the Maracaibo block moved northward and converged on the Paraguaná basement block (Blanco et al., 2013). The main source rock from the Falcon basin has been identified as the Agua Clara formation (Oligocene) and its main reservoir rocks include the Agua Clara and Socorro Formations (Oligocene-Miocene) (Yoris and Ostos, 1997).

Barinas-Apure basin. The Barinas-Apure basin is located in the southwestern part of Venezuela and is bounded by the Andes, the Serranía de Trujillo and the Baúl arch. This basin is a foreland basin parallel to the mountain front of the Merida Andes (Portilla, 1993). The main source rocks are the equivalent in age (Late Cretaceous) to the La Luna Formation (Navay formation). The main reservoir rocks are Escandalosa and Burguita Formations (Cretaceous) and its carbonate Guayacán Member (Yoris and Ostos, 1997).

Eastern Venezuela basin. The Eastern Venezuela basin (EVB) - the second most important hydrocarbon basin after the Maracaibo basin - is delimited by the Serranía de la Costa, the Orinoco River, the Orinoco Delta, and the Baúl Arch (Fig. 2B). The EVB represents a Neogene foreland basin overlying the Mesozoic passive margin of northern South America that was created during the oblique collision of the Caribbean plate with the northern edge of the South American continent (Di Croce, 1996; Escalona and Mann, 2011).

The EVB has been divided into two sub-basins: the Guárico and Maturín sub-basins (Fig. 2B). The Guárico sub-basin is located in the western area of the EVB and is bounded to the north by the Guárico thrust front (Fig. 2B). To the south, the EVB becomes less structurally complicated with the Espino rift preserving relatively undeformed Jurassic and Cambrian sedimentary rocks (Yoris and Ostos, 1997).

Changes in complexity of the Guarico sub-basin translate into the presence of four different petroleum systems in the area of the Espino rift: 1) Querecual-Oficina; 2) Temblador-La Pascua; 3) Querecual-Chaguramas; and 4) Oficina-Oficina with all four petroleum systems ranging in age from Cretaceous to Miocene (Yoris and Ostos, 1997).

The Maturín sub-basin is the main petroliferous basin to the east of the Espino rift (Fig. 2B). The Maturin sub-basin changes in complexity from the southern to its more deeply buried northern edge. To the north, thick sequences of Lower Cretaceous to Pleistocene are folded and thrusted while to the south there is a simpler stratigraphy - similar to the Guárico sub-basin (PDV Léxico, 1997). The main source rock of the Maturin sub-basin is the Querecual formation (Cretaceous), is twice the thickness of the La Luna formation to the west. Its main reservoirs rocks include the Carapita, La Pica, Oficina and Merecure (Miocene) Formations (Yoris and Ostos, 1997).

The Espino rift has been producing oil and gas from the Cenozoic formations (Oficina and Merecure) from the Cretaceous source rock of Canoa and Tigre. Precretaceous formations such as Ipire, Carrizal and Hato Viejo have showed to be bad quality reservoirs and source rocks with porosities of 1% and Total Organic Content (TOC) less than 1% (Varela, 2004).

2.3 DATA AND METHODS USED IN THIS CHAPTER

2.3.1 Geophysical and well data used in the study

Gravity and magnetic data. The gravity and magnetic analyses for this study were done using gravimetric anomaly and total magnetic intensity values generated by García (2009) and covering the entire area of Venezuela. These data were acquired during low-orbit satellite from the CHAMP and Grace satellite missions and using WGS84 as the map datum. The geopotential model used in this study combined the Pavlis et al. (2008) gravity compilation (i.e., EGM2008) developed in a least squares adjustment combining the ITG-Grace03S model, which was available to degree and order 180 along with its complete error covariance matrix - an equiangular grid and a resolution of 9.1 km. The magnetic compilation from Maus et al. (2009) is called EMAG2 and is a merge of, preexisting grids, ship, and airborne measurements. These used least squares collocation with anisotropic correlation function over the oceans, and substitutions of spherical harmonic degrees with the CHAMP satellite magnetic anomaly model MF6 with a resolution of 3.7 km (Maus et al., 2008).

A gravity anomaly reduction was done at mean sea level and the magnetic anomaly was projected to be an elevation of 4 km. The Bouguer correction was applied using a density of 2.67 g/cm^3. The data were compiled in the Bouguer Anomaly and Magnetic Anomaly Database of Venezuela using satellite, ship, and airborne magnetic information (Linares, 2013).

Refraction data. The refraction information used in this study was compiled from previous works published by Schmitz et al. (2008) in their contribution to the regional BOLIVAR-GEODINOS (Broadband Ocean Land Investigations of Venezuela and the Antilles Arc – Recent Geodynamics of the Northern Limit of the South American Plate) project. This project collected interdisciplinary geological and geophysical data from four deep seismic wide angle profiles. The arrival information from these profiles include upper crust and Moho detection. Bezada et al. (2010) generated an estimated depth to basement and depth to Moho maps for Venezuela. These maps were constructed using gravity anomaly data and were controlled by seismic refraction profiles and with previous interpretations (Feo-Codecido et al., 1984; Schmitz et al., 2002; Guedez, 2007; Christeson et al., 2008; Clark et al., 2008b; Magnani et al., 2009 and). The model was built using a grid size which varies between 42 and 56 Km. I used these maps to constrain the crustal thickness model for the region on the edge of the Espino rift.

Seismic reflection data. The seismic reflection data used in this study were provided by Ing. José Benavides of Petróleos de Venezuela S.A. (PDVSA) and consisted of five seismic transects with three of the transects at right angles to the trend of the Espino rift and two of the transects running parallel to the long axis of the rift (Fig. 4).

Figure 4. A. Location of three gravity transects, five seismic reflection transects, and five seismic refraction stations in the region of the Espino rift shown in green color from BOLIVAR-GEODINOS project (Schmitz et al., 2008). Subsurface faults bounding the Espino rift at depth are modified from Salazar (2006). Round circles on the gravity transects are locations of gravity measurements used for interpolation and depth estimates. B. Location of wells used for the gravity modeling and as ties to seismic reflection data are from Rios (2002) and Salazar (2006). Subsurface faults of the Espino rift are modified from Salazar (2006)

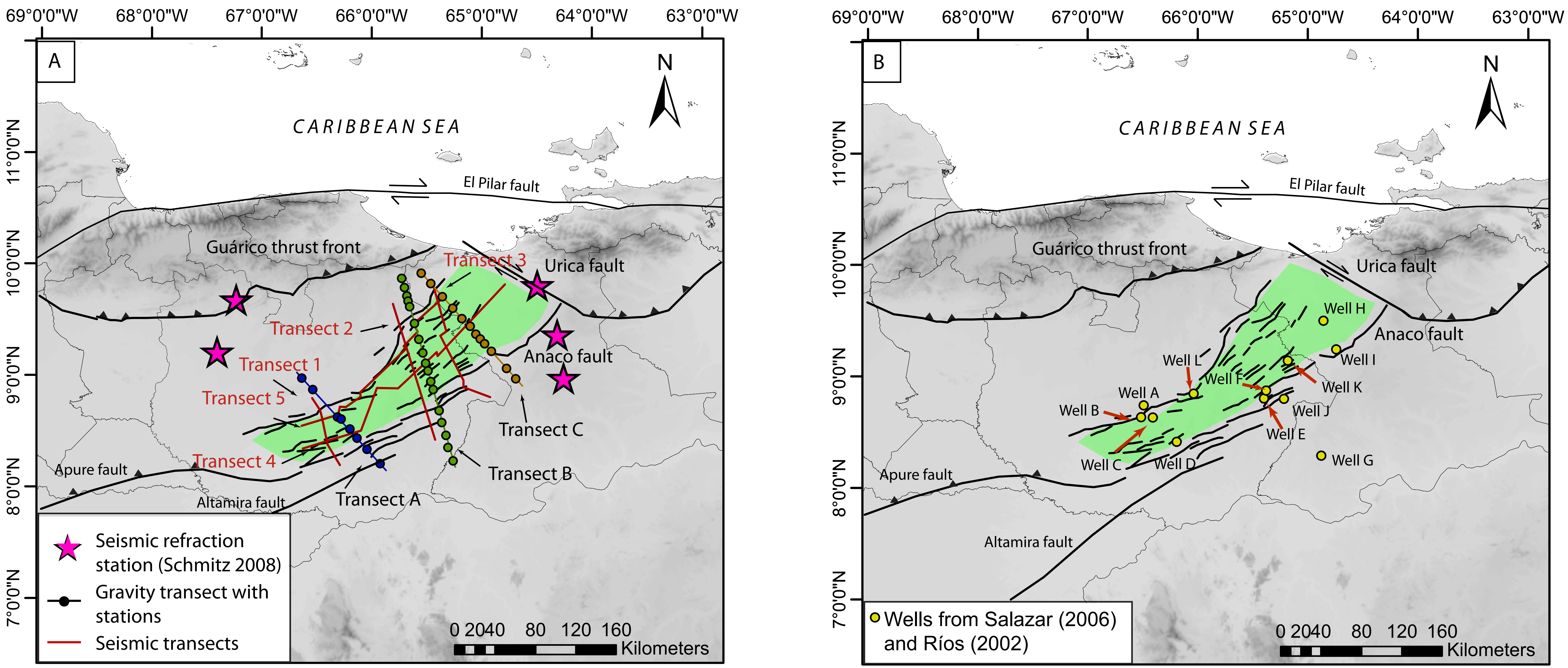

A
B
CARIBBEAN SEA
N
El Pilar fault
Guárico thrust front
Urica fault
Anaco fault
Apure fault
Altamira fault
Transect 1
Transect 2
Transect 3
Transect 4
Transect 5
Transect A
Transect B
Transect C
Seismic refraction station (Schmitz 2008)
Gravity transect with stations
Seismic transects
Well A
Well B
Well C
Well D
Well E
Well F
Well G
Well H
Well I
Well J
Well K
Well L
Wells from Salazar (2006) and Ríos (2002)
69°0'0"W
68°0'0"W
67°0'0"W
66°0'0"W
65°0'0"W
64°0'0"W
63°0'0"W
11°0'0"N
10°0'0"N
9°0'0"N
8°0'0"N
7°0'0"N
0 20 40 80 120 160
Kilometers

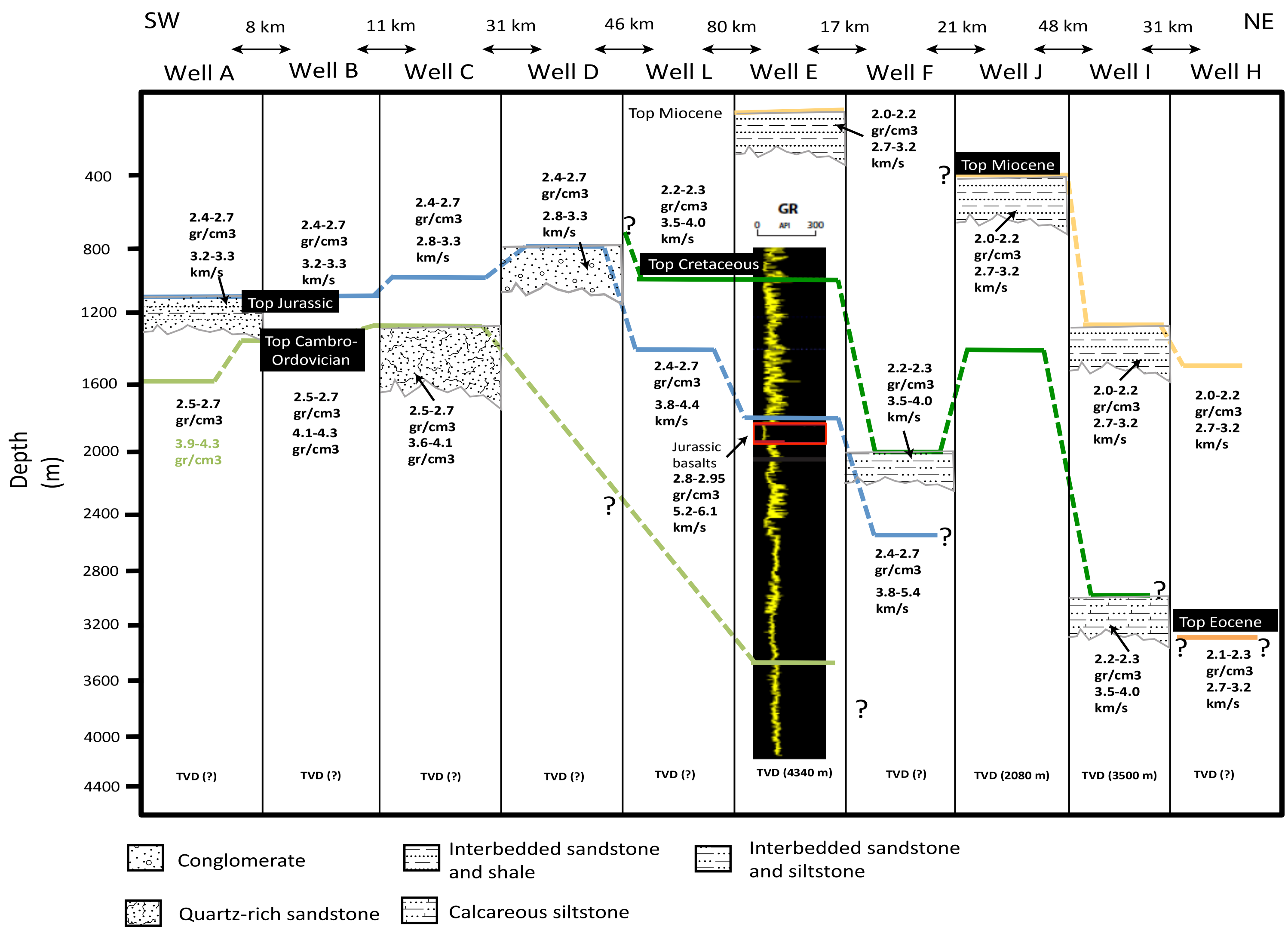

Figure 5. Well cross section from southwest to northeast along the axis of the Espino rift using well data compiled by Rios (2002), Varela (2004), and Salazar (2006)

Seismic data for all five transects were in two-way travel time with a maximum recorded depth of 6 s two-way time. These transects were assembled from various vintages of 2D and 3D seismic lines so some transects exhibit a better quality than others.

Well data. The well data used are industry wells published in Ríos (2002), Uzcátegui (2002), Varela (2004), Salazar (2006), and González (2006). Most of these wells penetrate the upper Paleozoic sedimentary fill of the Espino rift. However, the NZZ-88X well of Salazar (2006) (designated "Well E" in this study) encountered Jurassic basalts dated as late Jurassic in age (~160 Ma). All well data are summarized in Figure 5.

2.3.2 Methods used for analysis of gravity and magnetic data

Software and corrections. The gravity and magnetic database was loaded in Geosoft Oasis Montaj software to generate grids of the corrected Bouguer anomaly and Total Magnetic Intensity (TMI). Analysis of magnetic data was done using TMI and magnetic data reduced to the pole (RTP). TMI data provided information that allowed correlation to specific geological features known from outcrop mapping by previous workers.

Filtering. Filters applied to both gravity and magnetic data were used to: 1) suppress undesired signals from the shallower, basinal section and; 2) to reveal the desired signal related to the underlying basement of the Espino rift.

These enhancement techniques were useful for the interpretation of specific areas by removing the effects of noise and other, undesired signals. Enhancement included regional and residual calculations as well as deriving the analytic signal and total horizontal derivative of the tilt derivative calculated only for the magnetic data. These calculations included an upward continuation (10 km for the residual and 5 km for the analytic signal and the derivatives) in order to improve the desired signal and to better differentiate geological features.

Bouguer correction. The observed gravity data is a composite signal, which includes regional and residual information. The Bouguer correction is done to correct the observed gravity data for the height at which the data was measured and the topography (Lowrie, 2007). The Bouguer anomaly is related to the observed gravity data by:

$$gB = g_{obs} - g_{\lambda} + \delta_{gF} - \delta_{gB} + \delta_{gT} \qquad \text{(Equation 1)}$$

Where gB is the Bouguer anomaly, $g_{obs}$is the observed gravity, g_{λ} is the correction for latitude, δ_{gF} is the free-air correction, δ_{gB} is the Bouguer correction related to the gravitational attraction of rocks between the measurement and the sea level and δ_{gT} is the terrain correction (Lowrie, 2007). The Bouguer correction related to the gravitational attraction (δ_{gB}) can be obtained by:

$$\delta_{gB} = 2\pi\rho GH \qquad \text{(Equation 2)}$$

where ρ is the density of the material, G is the Universal Gravitational constant (6.67×10^{-11} N m^2 kg^{-2}) and H is the thickness of the plate (Lowrie, 2007).

Resolution of gravity and magnetic data. The gravity anomalies related to the regional gravity field generally reflect broad and regional features generated by large-scale sources. In contrast, the residual gravity field is related to more localized and buried features generated by smaller scale sources that can remain obscured until the regional field is removed (Gibson and Milligan, 1998). Similarly, the magnetic anomaly is the sum of all magnetic fields produced by different sources with small-scale sources embedded in the residual and large-scale sources embedded in the regional (Li and Oldernburg, 1996). These two signals can be separated and used separately for specific analyses of their sources.

Determining depth of sources. After anomaly separation, the signals can be related to individual sources depending on their relative depths. The calculation at various levels to the depth of a source can be done by field continuation and it will depend on the type of signal the interpreter wants to enhance (Blakely, 1995). Upward continuation transforms the potential field measured at one surface into some field measured at a higher surface. This method tends to attenuate anomalies related to local-near surfaces allowing the accentuation of deeper sources (Blakely, 1995). Oasis Montaj calculates the upward continued field through Fast Fourier Transform (FFT). The reciprocal relation of a Fourier Transform of a space domain function $f(x, y)$ is defined by:

$$f(x, y) = \frac{1}{4\pi^2} \int_{-\infty}^{\infty} \int_{-\infty}^{\infty} \overline{f}(\mu, v) - e^{i(\mu x + v y)}\, d\mu dv \qquad \text{(Equation 3)}$$

where μ and v are wavenumber in the x and y directions, respectively (Oasis Montaj 8.5.5, Manual).

When considering a gravity or magnetic grid that includes different sources, the depth of the top of the sources can be obtained using the following relationship:

$$logE(r) = 4\pi hr \qquad \text{(Equation 4)}$$

where h is the depth to the top of the source and r is the radial component in the wavenumber domain (Oasis Montaj 8.5.5, Manual). The upward continuation of a grid can then be calculated through:

$$L(k) = e^{-2\pi hk} \qquad \text{(Equation 5)}$$

where k is the wavenumber domain increment, used to depict a radially symmetrical variable (Oasis Montaj 8.5.5, Manual).

The downward continuation is fixed below the original observation level and it is used to enhance signals from shallow sources or short wavelengths (Blakely, 1995). Continuation is used for both gravity and magnetic data.

Analytic signal. Another method to enhance desired magnetic sources is using the analytic signal, or energy envelope. This type of filter is independent of the direction of magnetization of the source and its amplitude is related directly to the amplitude of magnetization (Macleod et al., 1993). The amplitude of the analytic signal can be obtained through this equation:

$$|A(x,y)| = \sqrt{\frac{\partial M^2}{\partial x} + \frac{\partial M^2}{\partial y} + \frac{\partial M^2}{\partial z}} \qquad \text{(Equation 6)}$$

where M is the observed magnetic field (Roest et al., 1992)

Derivatives. The last method used in this study to enhance the desired signal is derivatives, specifically the total horizontal derivative of tilt derivative (TDR_THDR). The TDR_THDR is an extension of the tilt derivate, which is used to delineate edges of bodies with vertical induced magnetization. Derivatives solve for the cases where the magnetization is not vertical. This type of derivative can be calculated as it follows:

$$TDR\ THDR = \sqrt{(\frac{\partial}{\partial x}TDR)^2 + (\frac{\partial}{\partial y}TDR)^2} \qquad \text{(Equation 7)}$$

Gravity transects. The gravity database was used to generate three gravity transects across the Espino rift using the GM-SYS application in Geosoft Oasis Montaj software (Fig. 4). The wells in the Espino rift were used to constrain the gravity model for its sedimentary section. Selected points from Bezada et al. (2010) were also used to constrain the depths to the basement and Moho in the area of the Espino rift.

Seismic reflection transects. Seismic interpretation of the five seismic reflection transects were constrained by wells compiled from previous studies and summarized on Table 1. These wells were used to integrate the three gravity profiles and the five seismic transects.

The seismic interpretation was done using Petrel software on a workstation. A total of 32 individual, 2D SEGY files were loaded by me in order to build the seismic transects shown in this thesis.

2.4 INTERPRETATION OF GRAVITY AND MAGNETIC DATA FROM THE ESPINO RIFT REGION

2.4.1 Application of filters and enhancements to regional gravity and magnetic data

Observed gravity and TMI. The observed gravity map shows a northern gravity maxima corresponding to the southern extension of the east-west-trending Great Arc of the Caribbean (GAC) (Fig. 6A). The GAC includes the islands of Aruba, Curacao, Bonaire, Las Aves, Los Roques, La Orchila, Nueva Esparta, La Tortuga, Los Testigos, and the Aves Ridge.

Moving to the south, the Maturín sub-basin shows a minimum in observed gravity centered on its sedimentary depocenter south of the frontal thrust bounding the Serrania del Interior (Fig. 6A). To the west of the Maturín sub-basin, along the Cordillera de la Costa, the observed gravity minimum is can be followed along the Guarico frontal thrust.

To the west of the Cordillera de la Costa a gravity minimum trends from north to northeast in the Sierra de Perijá, and the Venezuelan and Colombian Andes, respectively (Fig. 6A). The Maracaibo basin shows a gravity maximum that includes the Andes, the Sierra de Perijá and the GAC. The Eastern Venezuela basin show an extensive gravity maximum extending eastward to the Orinoco Delta.

Figure 6. Comparison of raw and residual gravity and magnetic data from the region of the Espino rift with overlay of major faults and crustal province boundaries from Ostos et al. (2005). Subsurface faults of the Espino rift are modified from Salazar (2006). Large black arrows indicate possible suture zone separating the Paleozoic orogenic belt to the northwest from the Precambrian shield to the southeast. **A**. Observed, regional gravity data; **B.** Zoom of observed gravity data from the area of the Espino rift; **C.** Observed, total magnetic intensity (TMI) data from the region; and **D.** Zoom of TMI data from the area of the Espino rift; **E.** Bouguer anomaly residual after upward continuation (10 km) in the region of the Espino rift; **F.** Zoom of Bouguer anomaly residual after upward continuation (10 km) in the area of the Espino rift; **G.** TMI residual after upward continuation (10 km) in the region of the Espino rift; **H.** TMI residual after upward continuation (10 km); **I.** Analytical signal of TMI after upward continuation (5 km) in the region of the Espino rift; **J.** Zoom of analytical signal after upward continuation in the area of the Espino rift; **K.** Tilt derivative of the total horizontal derivative after upward continuation (5 km) in the region of the Espino rift; and **L.** Zoom of tilt derivative of the total horizontal derivative after upward continuation (5 km) in the area of the Espino rift. **Key abbreviations: CL**=Caura lineament, **MS**=Maturín sub-basin, **GS**=Guárico sub-basin, **MB**=Maracaibo basin, **SP**=Sierra de Perijá, **SID**= Serranía del Interior, **MCH**= Machete fault, **RSF**=Ruíz-Sabán fault, **GSF**=Guama-Sabán fault, **AN**=Aníbal fault, **AF**= northeastern extension of the Altamira fault

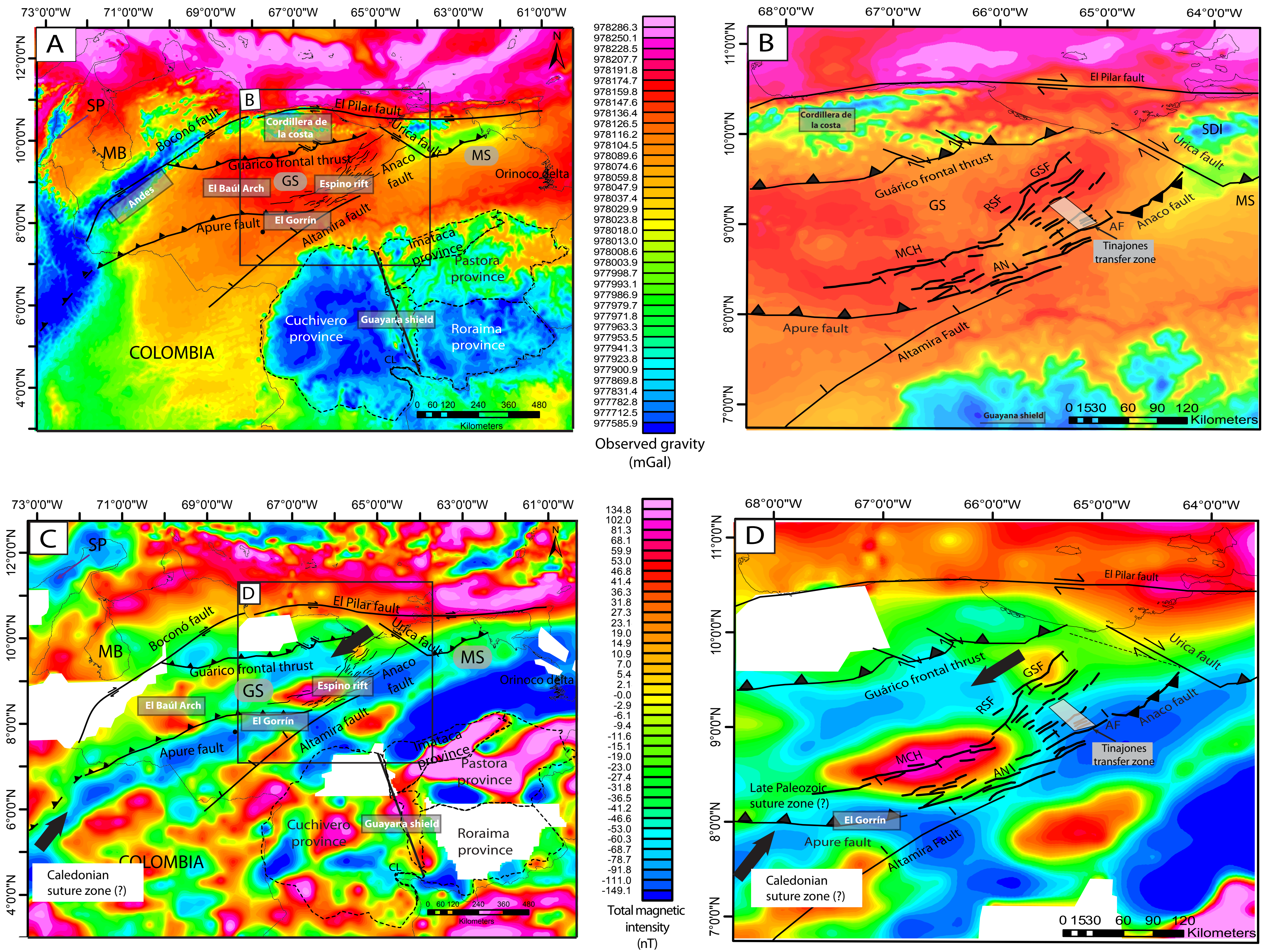
A
B
C
D
73°0'0"W
71°0'0"W
69°0'0"W
67°0'0"W
65°0'0"W
63°0'0"W
61°0'0"W
12°0'0"N
10°0'0"N
8°0'0"N
6°0'0"N
4°0'0"N
68°0'0"W
66°0'0"W
64°0'0"W
11°0'0"N
9°0'0"N
7°0'0"N
SP
MB
Boconó fault
El Pilar fault
Cordillera de la costa
Urica fault
Guárico frontal thrust
MS
Anaco fault
Orinoco delta
GS
El Baúl Arch
Espino rift
Andes
Apure fault
El Gorrín
Altamira fault
Imataca province
Pastora province
Cuchivero province
Guayana shield
Roraima province
CL
COLOMBIA
SDI
GSF
RSF
AF
Tinajones transfer zone
MCH
AN
Late Paleozoic suture zone (?)
Caledonian suture zone (?)
Kilometers
Observed gravity (mGal)
Total magnetic intensity (nT)

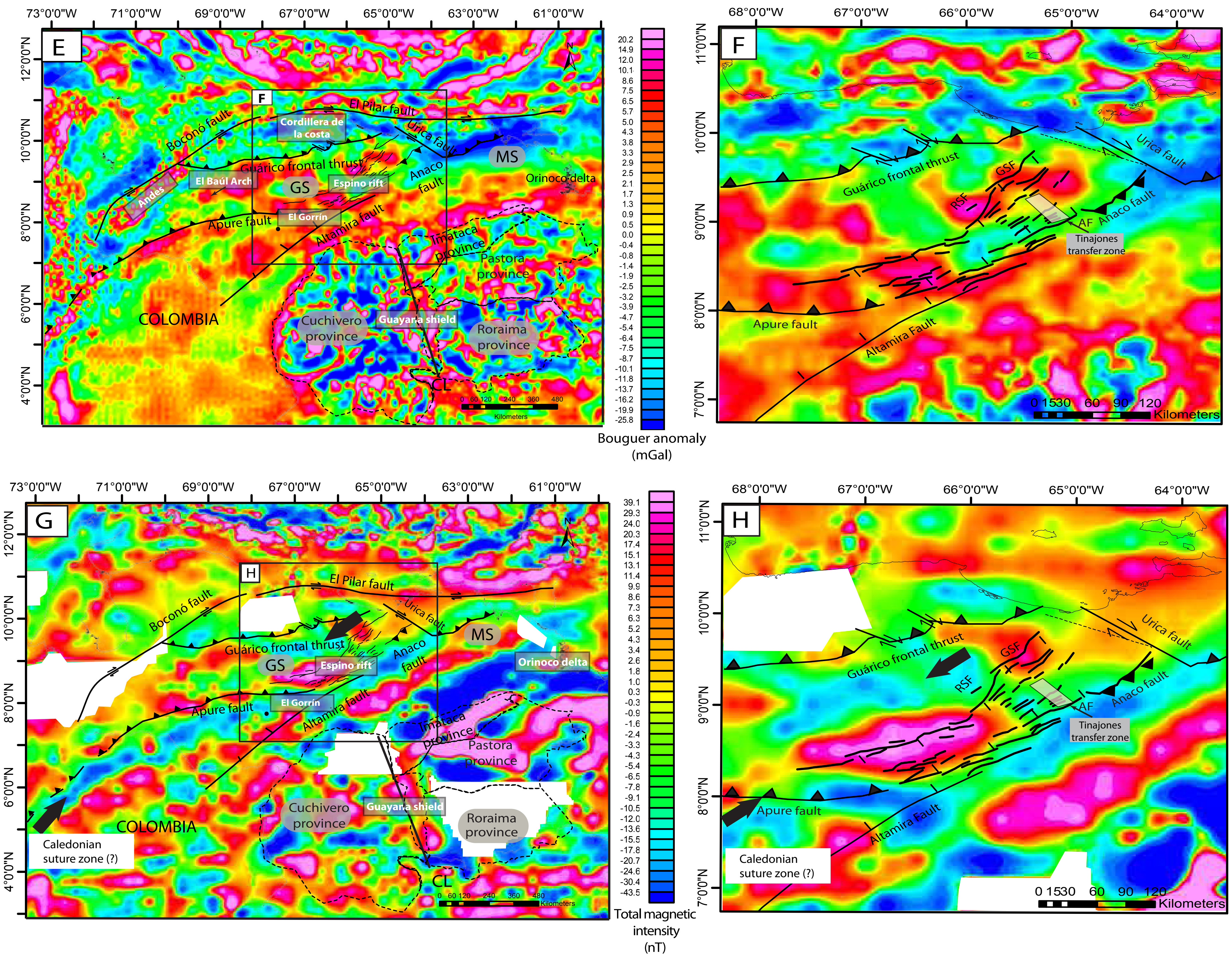
E
73°0'0"W
71°0'0"W
69°0'0"W
67°0'0"W
65°0'0"W
63°0'0"W
61°0'0"W
12°0'0"N
10°0'0"N
8°0'0"N
6°0'0"N
4°0'0"N
El Pilar fault
Cordillera de la costa
Boconó fault
Urica fault
MS
Orinoco delta
Guárico frontal thrust
Anaco fault
Andes
El Baúl Arch
GS
Espino rift
Apure fault
El Gorrín
Altamira fault
Imataca province
Pastora province
COLOMBIA
Cuchivero province
Guayana shield
Roraima province
CL
Kilometers
Bouguer anomaly (mGal)
F
68°0'0"W
67°0'0"W
66°0'0"W
65°0'0"W
64°0'0"W
11°0'0"N
10°0'0"N
9°0'0"N
8°0'0"N
7°0'0"N
Urica fault
Guárico frontal thrust
GSF
RSF
AF
Anaco fault
Tinajones transfer zone
Apure fault
Altamira Fault
0 15 30 60 90 120 Kilometers
G
El Pilar fault
Boconó fault
Urica fault
MS
Guárico frontal thrust
GS
Espino rift
Anaco fault
Orinoco delta
Apure fault
El Gorrín
Altamira fault
Imataca province
Pastora province
Cuchivero province
Guayana shield
Roraima province
COLOMBIA
Caledonian suture zone (?)
CL
Total magnetic intensity (nT)
H
Guárico frontal thrust
Urica fault
GSF
RSF
AF
Anaco fault
Tinajones transfer zone
Apure fault
Altamira Fault
Caledonian suture zone (?)
0 15 30 60 90 120 Kilometers

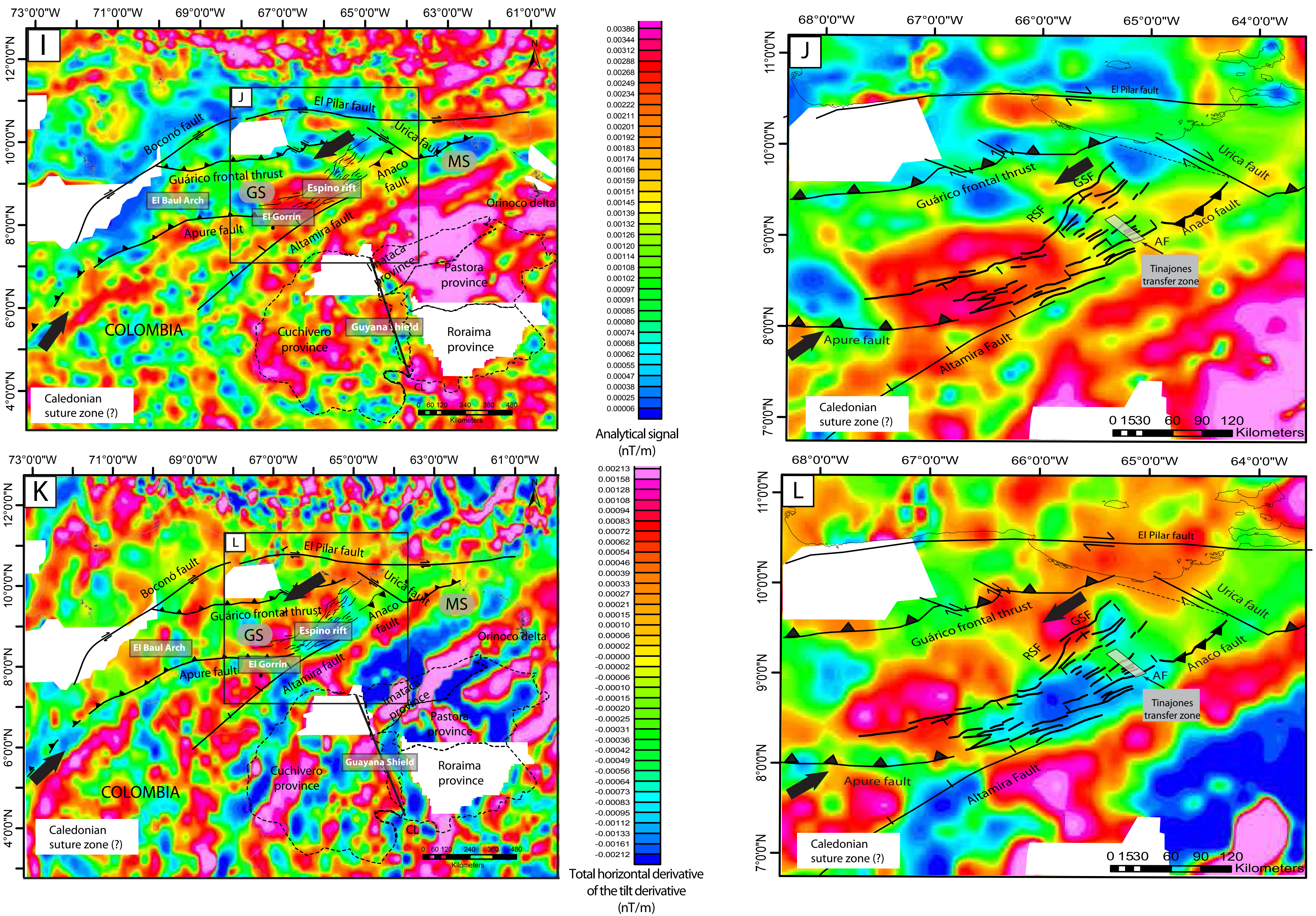

I
J
K
L
73°0'0"W
71°0'0"W
69°0'0"W
67°0'0"W
65°0'0"W
63°0'0"W
61°0'0"W
68°0'0"W
66°0'0"W
64°0'0"W
12°0'0"N
11°0'0"N
10°0'0"N
9°0'0"N
8°0'0"N
7°0'0"N
6°0'0"N
4°0'0"N
El Pilar fault
Boconó fault
Urica fault
Anaco fault
MS
GS
Guárico frontal thrust
Espino rift
El Baul Arch
El Gorrin
Apure fault
Altamira fault
Orinoco delta
Imataca province
Pastora province
COLOMBIA
Cuchivero province
Guyana shield
Guayana Shield
Roraima province
CL
Caledonian suture zone (?)
GSF
RSF
AF
Tinajones transfer zone
Kilometers
0 15 30 60 90 120
Analytical signal (nT/m)
Total horizontal derivative of the tilt derivative (nT/m)

The Guayana Shield, to the south shows an observed gravity minimum in the Cuchivero and Roraima provinces that changes to a gravity minimum to the east of the Caura lineament in the Imataca and Pastora provinces (Fig. 6A). This gravity minimum in the Cuchivero and Roraima provinces is related to the thicker crust (~40 km) beneath this part of the Guayana Shield (Schmidt et al., 2002). There are no prominent changes in observed gravity near the Espino rift. However, there are changes within the gravity maximum as revealed by increasing gravity in the northeastern and southwestern sections of the rift and a gravity minimum in the center of the rift. These effects likely reflect along-strike, thickening of the Espino rift from thinner in the southwest to thicker in the northeast (Fig. 6B).

Total magnetic intensity map. The total magnetic intensity (TMI) map shows anomalous magnetic lows along the northern boundary of the offshore GAC and highs along its southern bounday (Fig. 6C). This TMI map reveals mainly longer wavelengths because the shorter wavelengths are not visible at distances of 4 km above the sea level (García, 2009).

To the west a magnetic low is located in the Sierra de Perijá (Fig. 6C). East of the Sierra de Perijá, the Falcón basin, there is a magnetic high which extends to the western part of the Maracaibo basin. A magnetic low crosses the country in a northeasterly direction and closely follows the trace of the Apure fault, which bounds the Gorrín metamorphic belt, along its southwestern segment. The Gorrin metamorphic belt is composed of fine-grained rocks, pelitic hornfels with abundant biotite and metamorphosed tuffaceous sandstone overlaing Cretaceous sedimentary rocks (Feo-Codecido, 1984). The Apure fault forms the southern edge of the Gorrin metamorphic belt (south of the Machete fault) to the Barinas-Apure basin (specifically near San Fernando de Apure) and has been previously interpreted as the Caledonian suture zone separating Paleozoic orogenic belt of Venezuela and the Early Paleozoic sedimentary rocks or the Precambrian Guayana Shield (Feo-Codecido, 1984).

To the east, the Orinoco Delta shows a magnetic low that abruptly transitions to the south with a magnetic high produced by the Imataca and Pastora provinces, which are the oldest and thickest crustal provinces in the Guayana Shield and contain igneous intrusions (Korol, 1965; Hurley et al., 1973) (Fig. 6C). The younger Cuchivero province shows a magnetic high in its central area. The Imataca province shows a magnetic low to the southeast, which is related to an outcrop belt of magnetite which is characteristic of the Cuchivero province. (Figueroa et al., 2011)

In the Espino rift area, the Machete fault shows a magnetic high along its northeastern extension that is likely associated with shallower crystalline basement within the southwesterm part of the Espino rift (Fig. 6D). Along the northeast part of the rift, there is a magnetic low associated with the buried Aníbal normal fault and exposed and inverted Anaco thrust fault, which could be the northeastern extension of the Caledonian suture along the Apure fault as proposed by Feo-Codecido et al. (1984).

Residual maps after upward continuation (10 km). The Bouguer anomaly residual after upward continuation (10 km) shows a series of maxima in the GAC that alternates laterally with minima corresponding to the right-lateral, El Pilar strike-slip fault zone (Fig. 6E). South of the El Pilar fault the Cordillera de la Costa shows a gravity minimum which extends along the mountain belt and the Urica fault and includes the the Maturín sub-basin depocenter. This gravity minimum seems to end in the contact of the Guárico thrust front, where a gravity maximum is shown in the Guárico sub-basin and along the Apure and Altamira fault (Fig. 6E). On the Guayana Shield, the Cuchivero and Roraima provinces show similar gravity lows that alternate with gravity highs. These alternating gravity highs and lows contrast with the more uniform gravity high that characterizes the Imataca and Pastora crustal provinces.

The Espino rift shows in its northeastern and central sections a gravity minimum in the hanging wall of the Aníbal normal fault and a gravity maximum in the footwall block to the east (Fig. 6F). This gravity minimum is not apparent in the southern and northeastern part of the rift and it might be related to the basement being shallower in these areas than beneath the central rift

TMI residual map after upward continuation (10 km). The TMI residual after upward continuation (10 km) shows a magnetic low along the GAC. Along the Apure fault a magnetic low along its southeastern edge and a magnetic high along its northwestern edge is proposed to represent the change between the highly metamorphosed rocks of the Gorrín metamorphic belt and sedimentary rocks of the Barinas-Apure basin (Feo-Codecido, 1984) (Fig. 6G).

The Maturín sub-basin shows a magnetic low in its main depocenter and a magnetic high along its southern edge. The zoomed section shows a magnetic high along the Machete and Guama-Sabán fault followed by a magnetic low in the center of the rift (Fig. 6H). This could indicate a shallower source –i.e., basement and/or volcanic intrusions- in the bounding faults of the rift and a deeper source in the deepest section of the rift. The presence of the iron-rich basalts to the west of the Altamira fault could also be associated with the magnetic high (Mosticska, 1985). The presence of magnetic lows and high to the southeast of the Espino rift, and parallel to it, suggests a limit between older provinces present in the Guayana Shield and the younger orogenies to the northwest of the rift. This regional alignment of features indicates that limit proposes the Espino rift one segment of the Caledonian suture separating the Paleozoic belt to the northwest from the Precambrian Guayana shield to the southeast (Fig. 6H)

Analytical signal and Total horizontal derivative of tilt derivative. The analytical signal map shows a magnetic high to the north of the GAC followed by a transition zone of magnetic lows that extends southward to the El Pilar fault (Fig. 6I). Along the Apure fault a magnetic high that trend parallel to the metamorphic rocks of the Gorrín metamorphic belt (Feo-Codecido, 1984). The Imataca and Pastora provinces show a magnetic high that reflects differences in the mineral compositions of both provinces. North of the Imataca province there is a magnetic high with the same magnetic intensity as the Imataca province that supports the northward extension of the Imataca province as proposed by Ostos et al. (2005) (Fig. 6I).

The Cuchivero province contains a magnetic high to the northwest and magnetic lows to the southeast. The Espino rift (Fig. 6J) shows a magnetic high in the Machete and Altamira fault, which also extends into the central part of the rift and that may reflect the shallower basement in this area and/or the changes in lithologies within the rift's sedimentary fill (i.e. the Ipire formation with interbedded red beds).

Tilt derivative map. The total horizontal derivative of the tilt derivative map shows changes in magnetic responses laterally in the GAC (Fig. 6K). Along the Guárico frontal thrust a magnetic high is present and is likely controlled by the thrust fault. The Apure fault is defined between two magnetic highs, which can be related to the limit of the Gorrín metamorphic belt and younger Paleozoic sedimentary rocks (Ostos et al., 2005)

The Cuchivero province of the Guayana shield shows a magnetic high elongate in a northeast-southwest direction that contrasts with the low magnetic response in the surrounding region (Fig. 6L). This rapid change in the magnetic character can be associated with changes in sedimentary and meta-igneous rocks present in the south ern Guayana Shield (Gonzáles de Juana et al., 1980). The bounding faults of the Espino rift are better delineated using total horizontal derivative of the tilt derivative. From this filter, the Machete, Altamira Ruíz and Guama Sabán faults all show a magnetic high, which becomes less prominent in the deeper, central section of the rift which is characterized by a magnetic low (Fig. 6L).

2.4.2 2D gravity transects across the Espino rift

I used 2-D forward gravity models along transects approximately perpendicular to southwest to northeast main axis of the Espino rift to analyze the changes in crustal and upper mantle structure (Fig. 4A).

Figure 7. A. Gravity anomaly along gravity transect A crossing the southern end of the Espino rift characterized by thin, syn-rift sedimentary fill (location of transect shown in D); **B.** Gravity transect with pink stars showing tie points taken from depth to basement and depth to Moho maps from Bezada et al. (2010); **C.** Vertically-exaggerated zoom of the Espino rift taken from the gravity model and showing the densities used; and **D**. Map of the Espino rift in green showing location of gravity transect A (red line) crossing the southern end of the rift

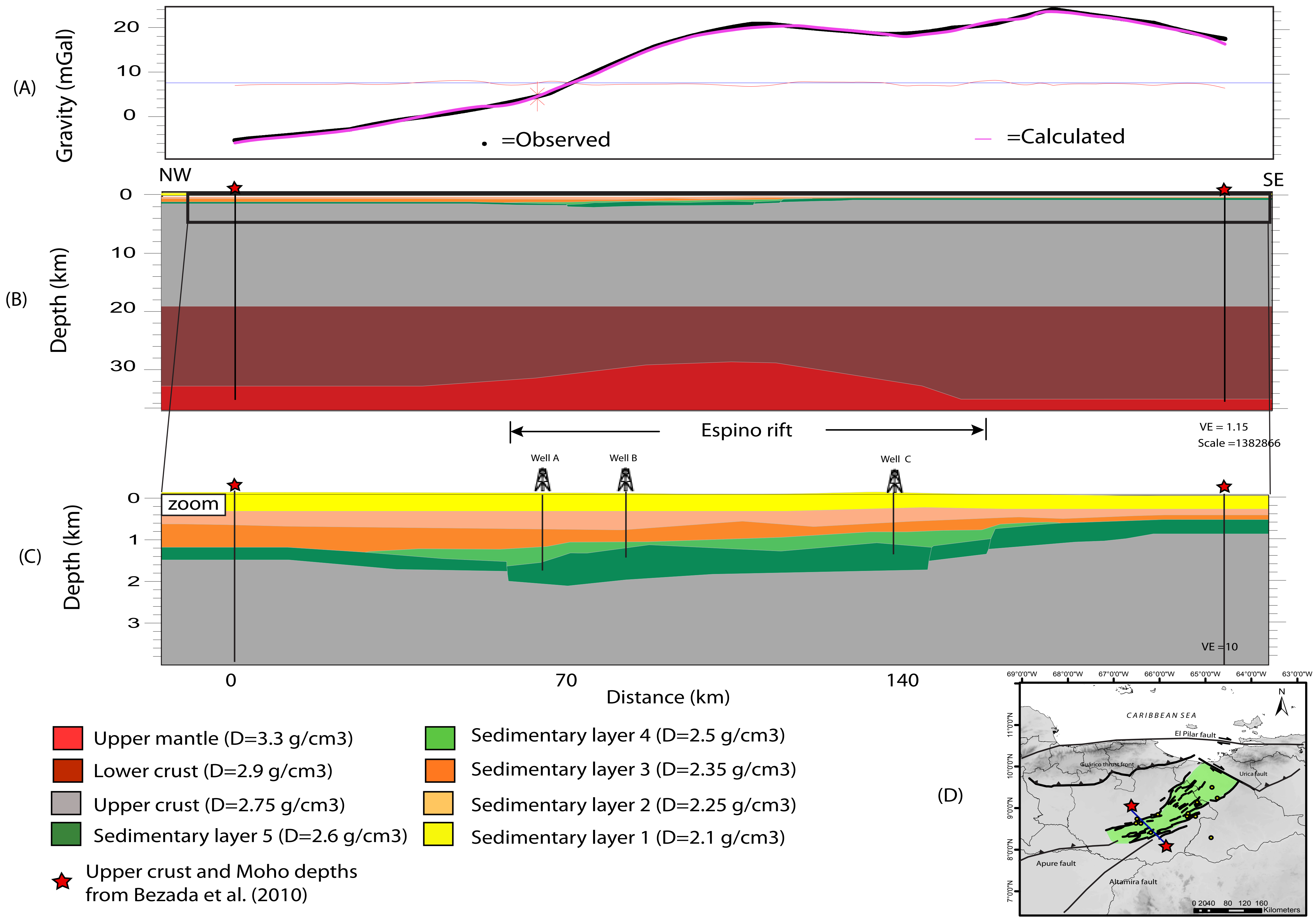

(A)
Gravity (mGal)
20
10
0
=Observed
=Calculated
(B)
NW
SE
Depth (km)
0
10
20
30
Espino rift
VE = 1.15
Scale =1382866
(C)
Depth (km)
Well A
Well B
Well C
zoom
0
1
2
3
VE = 10
0
70
140
Distance (km)
Upper mantle (D=3.3 g/cm3)
Lower crust (D=2.9 g/cm3)
Upper crust (D=2.75 g/cm3)
Sedimentary layer 5 (D=2.6 g/cm3)
Sedimentary layer 4 (D=2.5 g/cm3)
Sedimentary layer 3 (D=2.35 g/cm3)
Sedimentary layer 2 (D=2.25 g/cm3)
Sedimentary layer 1 (D=2.1 g/cm3)
Upper crust and Moho depths
from Bezada et al. (2010)
(D)
69°0'0"W
68°0'0"W
67°0'0"W
66°0'0"W
65°0'0"W
64°0'0"W
63°0'0"W
CARIBBEAN SEA
El Pilar fault
Guárico thrust front
Urica fault
Apure fault
Altamira fault
N
0 20 40 80 120 160
Kilometers

Gravity transects were selected to closely coincide with seismic reflection transects in order to constrain the shallow structure with seismic reflection, well, and geologic information. Gravity values were extracted from the compilation done by García (2009) and the model was constructed using topography information from the National Geophysical Data Center (NGDC).

The geometry of the gravity models was based on eight layers including five sedimentary layers, one upper and one lower crustal layer, and one upper mantle layer. For one of the models a local thin layer of basalt was included (Fig. 7). The five sedimentary layers represent sedimentary layer of Cambrian age to present related to the sediments deposited during the five tectonic phases of the Espino rift. For the upper crust and Moho layer the depths are available from previous gravity studies (Bezada et al., 2010) and refraction stations from the BOLIVAR-GEODINOS project (Schmitz et al., 2008). The boundary between the upper and lower crustal layer was fixed at a depth of 19 km for each transect to be consistent in my model. The lack of refraction stations near or within the Espino rift required me to use four points from Bezada et al. (2010) depth to basement and depth to Moho maps to constrain the ends of the gravity transects. For depth to basement and Moho maps (Fig. 10 and 11) refraction information from Schmitz, et al., (2008) was included to interpolate the maps beyond the limits of the Espino rift.

The densities used for each layer were the same for the three transects to be consistent with the models. Densities used for the five sedimentary layers were based on density and well log information compiled from of Ríos (2002), Salazar (2006), Jácome et al. (2008), and González (2009) (Fig. 3 and 5). According to previous work, Oligocene to present sediments (foreland basin) could be associated with Sedimentary layer 1 (2.1 g/cm^3) and Sedimentary layer 2 (2.25 g/cm^3), Late Jurassic to Cretaceous sediments (passive margin and post Jurassic rifting fill) correspond to Sedimentary layer 3 (2.35 g/cm^3) and Sedimentary layer 4 (2.5 g/cm^3) Cambrian to Early Jurassic (syn-Jurassic rift fill and Cambrian formations of Carrizal and Hato Viejo) correspond to Sedimentary layer 5 (2.6 g/cm^3), along with upper crust (2.75 g/cm^3), lower crust (2.9 g/cm^3), and upper mantle (3.3 g/cm^3). Densities for basalt intrusions (2.85 g/cm^3) were obtained from well log data from Well E published by Salazar (2006) (Fig. 5).

Three gravity transects were made using data from the Bouguer Anomaly Database (García, 2009) that were gridded using program GM-SYS contained within Oasis Montaj software (Fig. 4). The average distance between the three gravity transects is 90 km and the three transects are roughly perpendicular to the southwestern, central, and northeastern parts of the Espino rift.

The Bouguer anomaly map forms the basis of the three transects and shows the contrast in density between the upper/lower crust and the mantle. The structure of the rift is obscured by the anomaly associated with its underlying mantle. The main objectives from my gravity modeling are to determine crustal thinning, depth to basement, and the depth to Moho.

Transect A: Southwestern Espino rift. Gravity transect A trends for a distance of 130 km in a northwest direction across the southwestern Espino rift (Fig. 4A). Crustal thickness within the rift ranges from 24 km to 28 km and increases to 30 km where there is little deformation on the flanks of the rift. The information that I used to constrain the thicknesses of the layers in this model included the top of major units in wells A, B and C shown in Figure 5. Additionally, I used two depth to basement and depth to Moho points from Bezada et al. (2010) at the northwestern and southeastern ends of gravity transect.

The zoomed section shows a thickness in the first layer, Sedimentary layer 1, of ~400 m, represents the upper part of the foreland basin phase (Ríos, 20002) (Figure 7A).

Sedimentary layer 2 layer shows thickness ranges of 500 to 250 m in a line from northwest to southeast. This layer reflects sedimentation within the foreland basin and passive margin settings (Ríos, 2002).

Sedimentary layer 3 layer shows thicker sections to the northwest (500 m) and thinner sections to the southeast. This layer records the passive margin setting (top) and final stage of the Jurassic rifting (base).

Sedimentary 4 show thickness of 400 m on the edges of the rift and 200 m in the central part. This thinning is attributed to a possible inverted structure in the southern section of the rift and in the top section of the Sedimentary layer 5.

Sedimentary layer 5 shows the thickest section in the center of the Espino rift and is associated with the inverted Altamira structure and the Machete fault (Feo-Codecido, 1984; Salazar, 2006). The sedimentary layer 5 is could be associated with the early stages of Jurassic rifting (Ríos, 2002) and Cambrian rifting and was terminated by the late Paleozoic collisional event.

Transect A shows that the Espino rift is a symmetrical graben with a thicker sediment column to the northwest, which is partly related to Cenozoic, foreland basin filling.

Transect B: Central Espino rift. Gravity transect B trends northwest over a distance of 190 km (Fig. 8). The information to constrain the thicknesses of the layers in this model was formation tops from wells D, E and F as shown in Figure 5. Additionally, one depth to basement and depth to Moho point extracted from Bezada et al. (2010) was included at the northwestern limit of the gravity transect. The crustal thickness beneath the rift ranges from 15 km to 19 km, and it increases to 25-28. The greater crustal thickness of transect B (Fig. 8) compared to transect A (Fig. 7) can be attributed to superposition of the Jurassic rift on top of the older, Cambrian rift in this location.

Sedimentary layer 1 layer has a thickness of ~700 m and forms the upper part of the Cenozoic foreland basin phase the upper part of the foreland basin phase (Ríos, 2002), and shows a thicker section compared to Fig. 6, affirming the thickening of syn-rift sedimentary rocks towards the rift axis.

Sedimentary layer 2 layer shows a thickness range from 1000 m in the northwestern Espino rift, to 1300 m in the center, to 600 m in the southeastern part of the rift. This layer is associated with the foreland basin and passive margin phase (Rios, 2002)

Figure 8. A. Gravity anomaly along gravity transect B crossing the central part of the Espino rift and characterized by an intermediate thickness of syn-rift, sedimentary fill (location of transect shown in D); **B**. Gravity transect with pink stars showing tie points taken from depth to basement and depth to Moho maps from Bezada et al. (2010); **C.** Map of the Espino rift in green shading showing location of gravity transect B (red line) crossing the southern end of the rift

Transect B

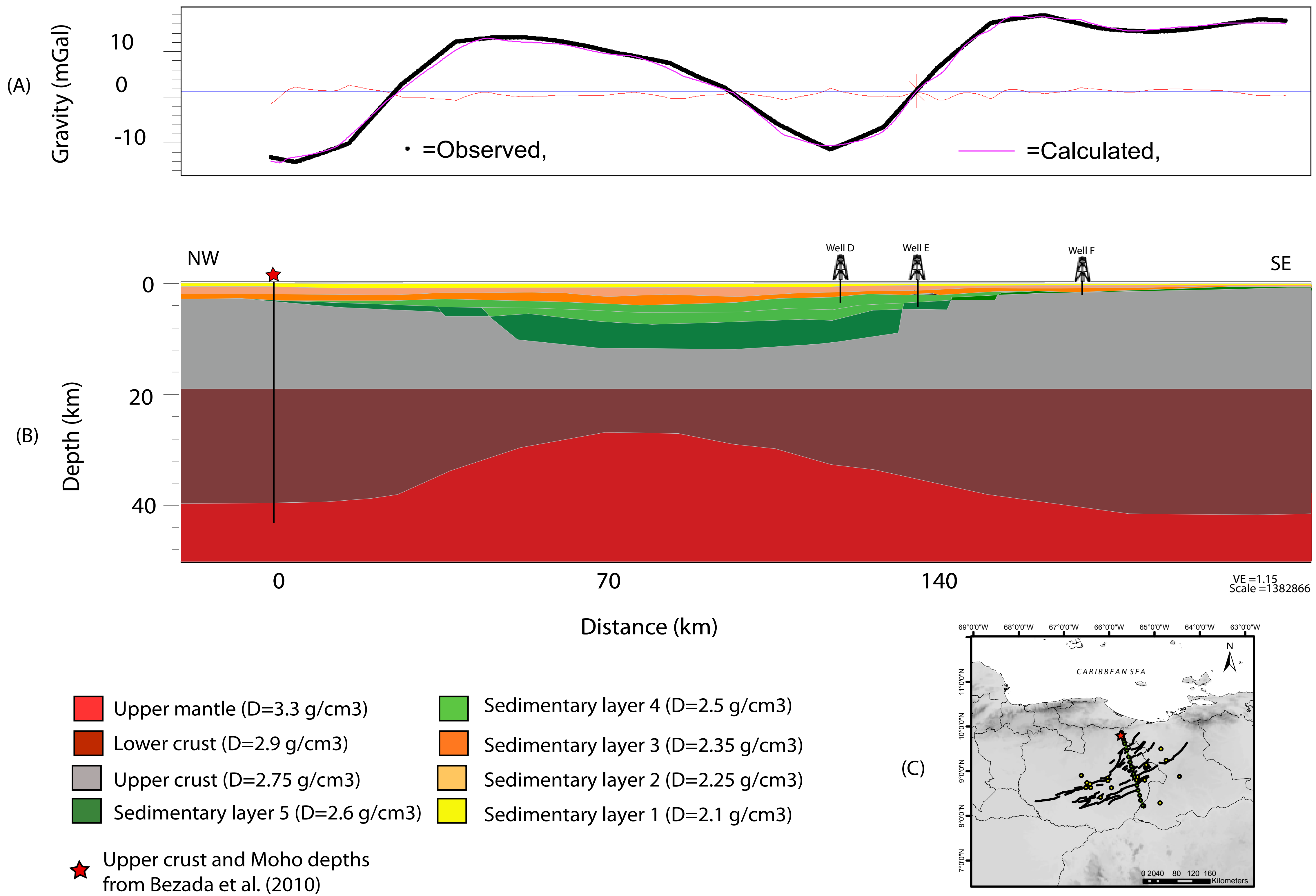
(A)
Gravity (mGal)
10
0
-10
• =Observed,
=Calculated,
(B)
Depth (km)
NW
SE
Well D
Well E
Well F
0
20
40
0
70
140
VE =1.15
Scale =1382866
Distance (km)
Upper mantle (D=3.3 g/cm3)
Lower crust (D=2.9 g/cm3)
Upper crust (D=2.75 g/cm3)
Sedimentary layer 5 (D=2.6 g/cm3)
Sedimentary layer 4 (D=2.5 g/cm3)
Sedimentary layer 3 (D=2.35 g/cm3)
Sedimentary layer 2 (D=2.25 g/cm3)
Sedimentary layer 1 (D=2.1 g/cm3)
Upper crust and Moho depths
from Bezada et al. (2010)
(C)
CARIBBEAN SEA
N
Kilometers

Sedimentary layer 3 shows thicker sections in the central part (1800 m) and thinner sections along the edges of the rift with a 1000 m thickness to the northwest and an 800 m thickness to the southeast. The upper part of this layer is associated with the passive margin and the lower part is associated with the Jurassic rift phase.

Sedimentary layer 4 show thickness of 4500 m in the central part of the rift. Layer 4 decreases to 500-2000 m on the flanks of the rift. This layer also includes a Jurassic basaltic flow correlative to the basalts found in Well E (Mostiscka, 1985) (Fig. 5). According to Ríos (2002) and Salazar (2006) the Jurassic, basaltic flows are localized to this area.

The deepest sedimentary layer (Sedimentary layer 5) shows the thickest section of the rift and is associated with the early stages of the Jurassic rifting (Ríos, 2002) and the underlying Cambrian rift fill. This section has a maximum thickness in the sedimentary fill of the rift of 3800 m, which decreases on the rift flanks to 1100 m. Fiorillo et al. (1981) used VSP information from Well E (NZZ-88X) to calculate a thickness estimate of the Cambrian-Ordovician (Carrizal and Hato Viejo formation) sediments. The average thickness is approximately 1.2 km according to the VSP data. We can assume that these sediments will have greater thickness in the rift axis.

Transect C: Northeastern Espino rift. Gravity transect C trends to the northwest across the Espino rift over a distance of 150 km. The information used to constrain the thicknesses of the layers in this model is based on well top data from wells G and H shown in Fig. 5. Additionally, one depth to basement and top Moho point was extracted from Bezada et al. (2010) was included at northwestern end of the gravity transect.

Figure 9. A. Gravity anomaly along gravity transect C crossing the northern part of the Espino rift characterized by an intermediate thickness of syn-rift, sedimentary fill (location of transect shown in D); **B.** Gravity transect with pink stars showing tie points taken from depth to basement and depth to Moho maps from Bezada et al. (2010); **C.** Map of the Espino rift in green showing location of gravity transect B (red line) across its northern end.

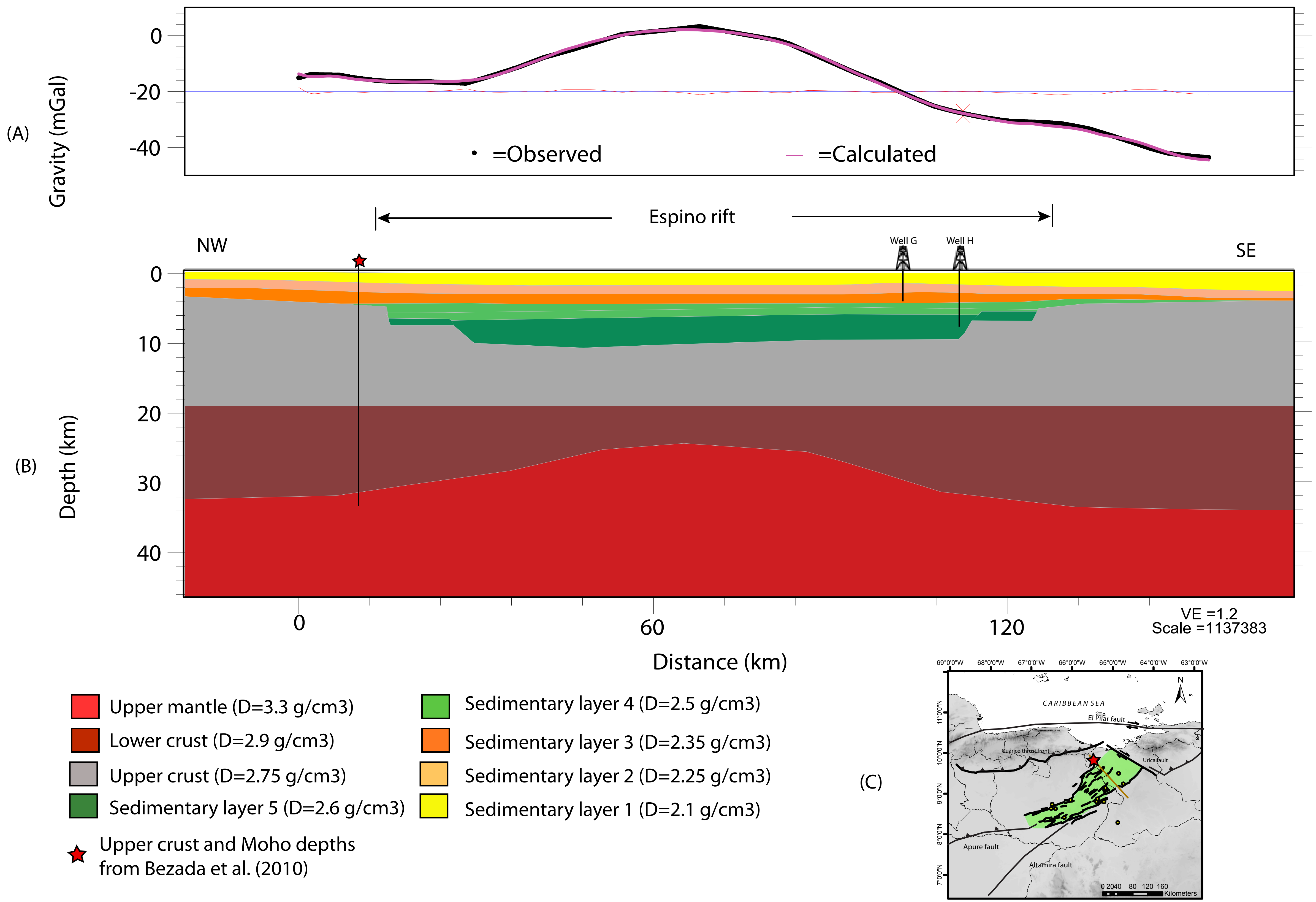
(A)
Gravity (mGal)
0
-20
-40
=Observed
=Calculated
Espino rift
NW
SE
Well G
Well H
(B)
Depth (km)
0
10
20
30
40
0
60
120
Distance (km)
VE =1.2
Scale =1137383
Upper mantle (D=3.3 g/cm3)
Lower crust (D=2.9 g/cm3)
Upper crust (D=2.75 g/cm3)
Sedimentary layer 5 (D=2.6 g/cm3)
Sedimentary layer 4 (D=2.5 g/cm3)
Sedimentary layer 3 (D=2.35 g/cm3)
Sedimentary layer 2 (D=2.25 g/cm3)
Sedimentary layer 1 (D=2.1 g/cm3)
Upper crust and Moho depths
from Bezada et al. (2010)
(C)
CARIBBEAN SEA
El Pilar fault
Urica fault
Apure fault
Altamira fault

The crustal thickness beneath the rift ranges from 14 km to 19 km and increases to 24-25 km. Similarly, the changes in crustal thickness of transect C (Fig. 9) compared to transect A (Fig. 7) can be related to thelocalized inversion of Cambrian normal faults during latest Jurassic rifting.

Sedimentary layer 1 layer has a thickness of ~2000 m and is associated with the upper part of the foreland basin phase (Ríos, 20002), with a thicker section compared to Transects A and B (Figs. 5 and 6).

Sedimentary layer 2 shows thickness ranges of 2200 to the northwest and to 1000 m to the southeast. This layer is associated to part of the foreland basin and passive margin phase (Ríos, 2002).

Sedimentary layer 3 shows thicknesses up to 2000 m in the central part that are associated with the passive margin phase (upper part) and Jurassic rifting phase (lower part). Sedimentary layer 4 show thickness of 2200 m to the NW and the central part of the rift and 2000-1200 m along the edges of the rift.

The deepest sedimentary layer 5 shows the thickest section of the rift and could be associated with the early stages of Jurassic rifting (Ríos, 2002) and earlier Cambro-Ordovician rifting event. This section has a maximum thickness of sedimentary fill of the rift of 4100 m. The interpreted thickness of layer 5 is consistent with the observed thickness of the same unit as seen on the seismic reflection data shown on Transect B.

In general, the three transects show thicker sedimentary sections in the central part of the profile, as expected from the general structure of the Espino rift. Transect B shows a much thicker section than the other two, suggesting that there was more intensive, Jurassic rifting in this area (Fig. 8). Crustal thicknesses decrease from southwest to northeast.

The level of changes in gravity anomaly in the gravity transects (panel A in figure 7, 8, and 9) can be associated with changes in deep sources (i.e., depth to the upper mantle) which changes along the length of the Espino rift.

2.4.3. Depth to basement beneath the Espino rift

The depth to basement (Fig. 10) and depth to Moho (Fig. 11) maps were generated from the three gravity models (Fig. 7, 8, and 9) and by using the top of the upper crust surface as top of crystalline basement and based on five refraction stations (Schmitz et al., 2008). The points were interpolated using Minimum Curvature in Oasis Montaj.

Depth to basement map (Fig. 10) shows a shallower basement in the southwestern part and deepens to the northeast. The deepest area of basement in the central part of the rift at a depth of 13 km reflects the area of maximum stretching and syn-rift fill in the Paleozoic and Jurassic combined with deep burial beneath the Cenozoic sedimentary rocks of the Eastern Venezuelan foreland basin.

2.4.4 Depth to Moho beneath the Espino rift

The depth to Moho map shows an elongate, northeast-striking high in the Moho beneath the central part of the Espino rift indicating elevated mantle beneath t he

Espino rift (Fig. 11). The central and northeastern gravity transect shows the top of the Moho at a depth of 25 km indicating the area of the Espino rift where the Moho is shallowest and the crust is thinnest. This indicates superimposed Cambrian and Jurassic rifting led to more extension in the central and northeastern parts of the Espino rift. Along the southwestern end of the Espino rift, the rift was not extensively reactivated during the Jurassic.

2.5 INTERPRETATION OF SEISMIC REFLECTION AND WELL DATA FROM THE ESPINO RIFT

My interpretation of the structure and stratigraphy of the Paleozoic and Jurassic, syn-rift fill of the Espino rift was done using five seismic reflection transects parallel to (Fig. 16 and 17) and at right angles to (Fig. 12, 13, and 15) long axis of the Espino rift. This interpretation was done using seven wells that were incorporated in the gravity modeling (Figs. 7, 8, and 9). The quality of the seismic data in the shallower section is average and deteriorates in the deeper, rift sections. Gain attributes were used before the interpretation to enhance the signal. The transects perpendicular to the Espino rift are separated by about 100 km while the transects parallel to the rift are separated by about 45 km (Fig. 4A).

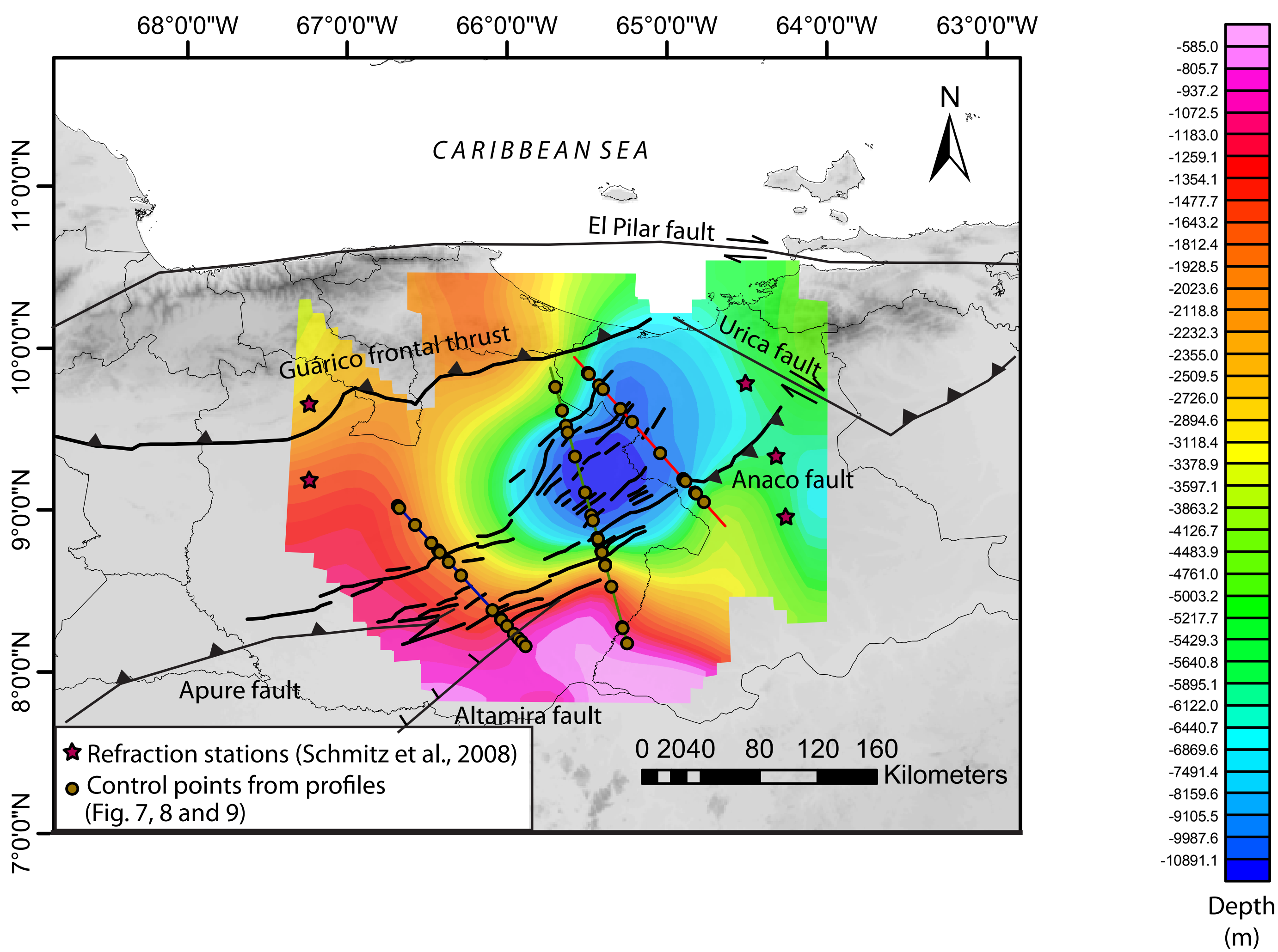

Figure 10. Depth to basement map from gravity profiles and refraction stations based on data from the BOLIVAR-GEODINOS project as interpreted by Schmitz et al. (2008). The north-central part of the rift characterized by the deepest sedimentary fill of the entire rift

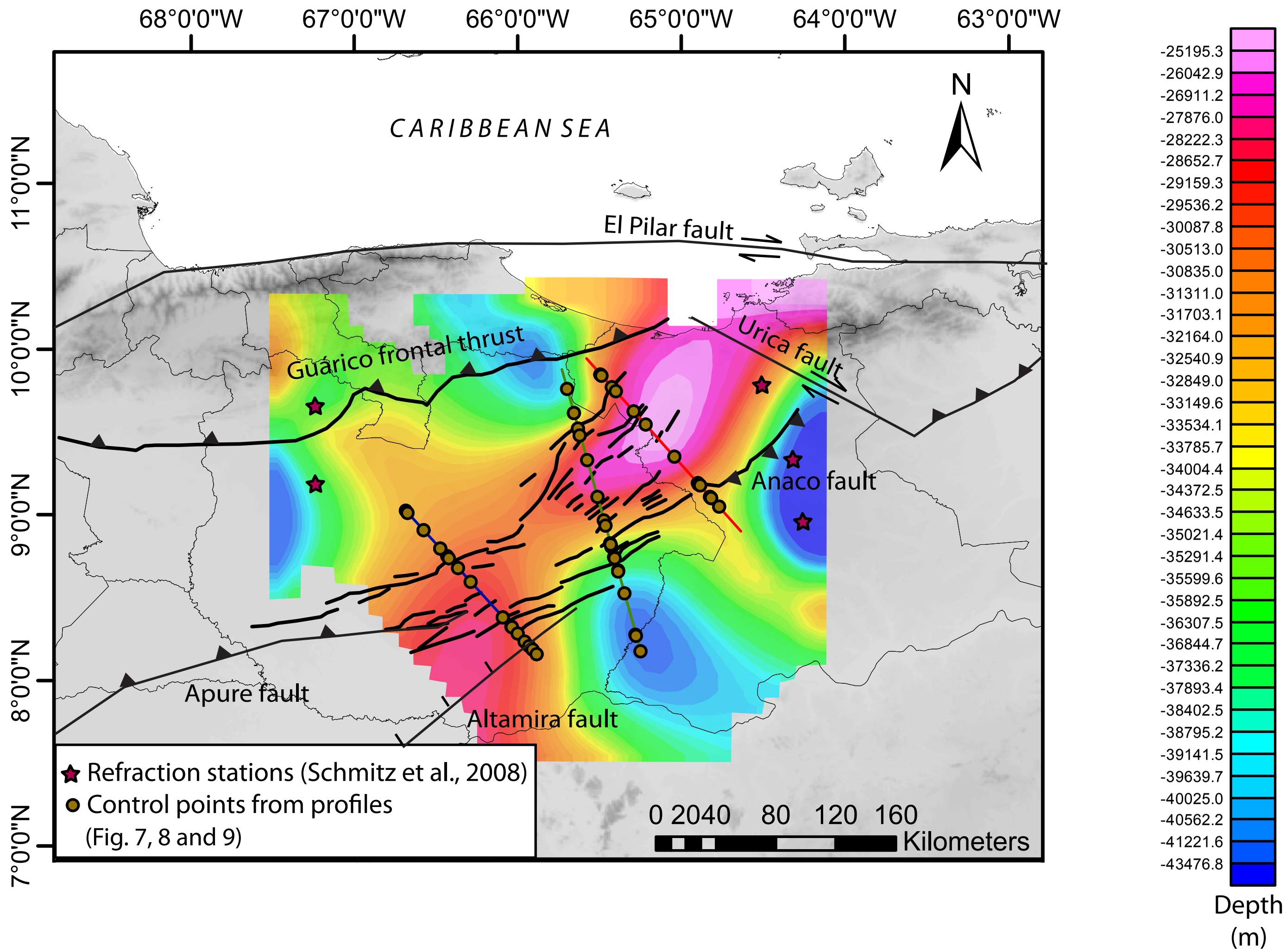

Figure 11. Depth to Moho map based on gravity profiles and refraction stations from the BOLIVAR-GEODINOS project as interpreted by Schmitz et al. (2008). The map shows that the thinnest, rifted crust is found in the north-central part of the rift

2.5.1 Seismic transect 1 orthogonal to the Southern Espino rift

Seismic transect 1 extends 95 km in a northwest to southeast direction and almost perpendicular to the bounding fault of the southwestern Espino rift (Fig. 12). The Machete and Altamira faults are thick-skinned, listric normal faults that penetrate Precambrian basement and deform rocks as young as the Paleogene. Salazar (2006) proposed that the normal faults bounding the Espino rift were low-angle normal faults and with one normal fault much greater in throw than the other bounding, normal fault and therefore framing an asymmetrical, half-graben structure. In my interpretation, I show the Espino rift as a more symmetrical, full-graben with differing vertical throws on the normal faults bounding the rift. (Fig. 12).

Wells shown on Figure 12 demonstrate that the Paleozoic section is thin in this part of the southwestern Espino rift (~200 m) and that this thin, syn-rift sedimentary fill contrasts with sections to the northeast where the Paleozoic syn-rift fill becomes much thicker (~500 m). The Jurassic section shows an abrupt thinning against both edges of the Altamira high (Fig. 12).

The Altamira high is as an inverted structure that deforms both the Paleozoic rift fill and the overlying Jurassic rift with no apparent, structural discordance between the two rift-fill sequences (Fig. 12). On seismic transect 1, faults along the northwestern edge of the Altamira high and along the edges of the rift deform rocks as young as Paleogene indicating of Mesozoic and Cenozoic reactivation of the older Paleozoic and Jurassic normal faults (Fig. 12).

Figure 12. A. Uninterpreted seismic data from seismic transect 1 crossing the southern end of the Espino rift characterized by the thinnest, syn-rift sedimentary fill. Well ties shown are summarized in Figure 5. **B.** Interpreted seismic data from seismic transect 1. In this area, the Espino rift is a full graben with a pronounced, domal high in its central area that deforms both the older Paleozoic rift and the younger, conformable Jurassic rift. Only a thin section of the Jurassic rift is preserved across the top of the high. Major, bounding normal faults of the Espino rift (Machete and Altamira) show listric shapes on seismic profiles and were previously mapped by Salazar (2006). Thickening along these normal faults is more pronounced for the Jurassic rift than the Cambrian-Ordovician rift. **C.** Map of the Espino rift in green showing location of seismic transect 1 (red line) across the southern end of the rift

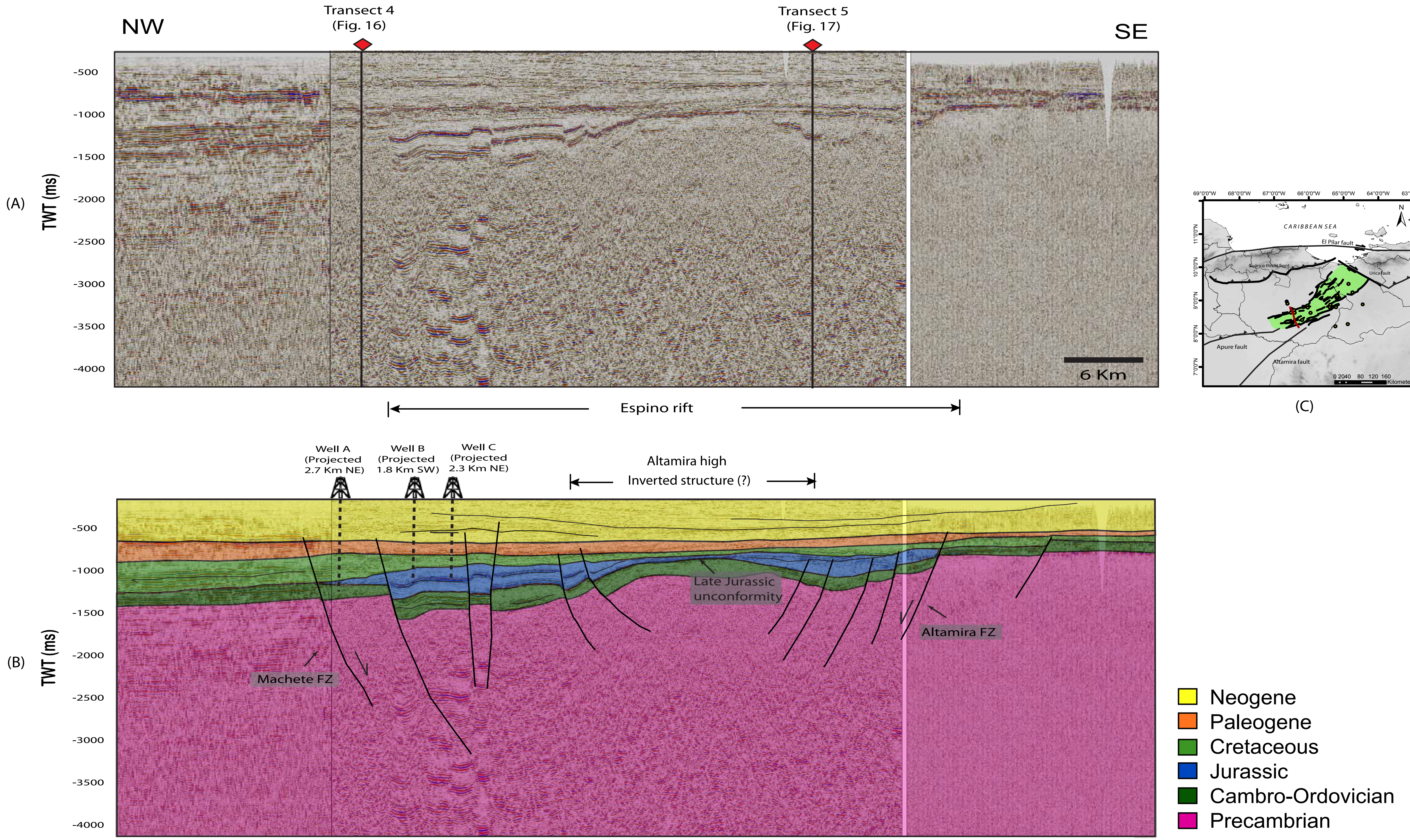

NW
SE
Transect 4 (Fig. 16)
Transect 5 (Fig. 17)
(A)
TWT (ms)
-500
-1000
-1500
-2000
-2500
-3000
-3500
-4000
6 Km
Espino rift
(C)
CARIBBEAN SEA
El Pilar fault
Apure fault
Altamira fault
Well A (Projected 2.7 Km NE)
Well B (Projected 1.8 Km SW)
Well C (Projected 2.3 Km NE)
Altamira high
Inverted structure (?)
(B)
Late Jurassic unconformity
Machete FZ
Altamira FZ
Neogene
Paleogene
Cretaceous
Jurassic
Cambro-Ordovician
Precambrian

There are three possible explanations for the angular unconformity present at the top of the Jurassic syn-rift section and within the interval of the upper part of the Jurassic syn-rift section.The first possibility is that these unconformities represent a "breakup unconformity" formed at the transition between rift-related normal faulting and the passive margin phase of the early Cretaceous that is characterized by the lack of normal faulting. This type of unconformity is related to the erosional beveling of the normal-fault bounding rift blocks as normal faulting ends as described in detail by Nottvedt et al. (1995) in the North Sea area. The second possibility for the unconformities present at the top of the late Jurassic section is the occurrence of a discrete, deformational event that produced the observed broad folds and inverted normal faults. I note support for both models in the descriptions below. The third possibility is that the folds are rollover type structures related to normal growth faults (Salazar, 2006). The third possibility seems the least likely explanation for the deformation in Transect 1 (Fig. 12) as the unconformities are mainly concentrated at the top of the syn-rift, Jurassic section rather than being more evenly distributed through the entire, syn-rift, Jurassic section.

Seismic transect 1 crosses the Machete area which forms the western part of the Orinoco Heavy-Oil Belt (Martínez, 1987) (Fig. 2B). The Altamira high within the Espino rift forms a structural boundary between the southern and southwestern zones of the Orinoco Heavy-Oil Belt which is expressed in the overlying clastic rocks of Cenozoic age (Galavis and Velarde, 1967; Vega and Rojas, 1987) (Fig. 2B).

2.5.2 Seismic transect 2 orthogonal to the Central Espino rift

Seismic transect 2 extends 140 km across the central part of the Espino rift which displays the greatest thickness of syn-rift Paleozoic and Jurassic fill (Fig. 13). The Ruíz-Sabán normal fault represents the northwestern limit of the Espino rift and Guama-Sabán normal fault shows a more east-west strike than the more northeasterly strike of most of the other normal faults bounding the central Espino rift. The Ruíz-Sabán fault penetrates downward into the Precambrian basement of the rift and penetrates upward into the late Cenozoic section showing that fault inversion was likely the result of the Cenozoic, oblique collision between the Caribbean and South American plates.

The Aníbal fault shows a minor, normal fault throw but the unnamed normal fault to the northwest shows a much larger, normal throw that records early Paleozoic growth faulting along this part or the Espino rift (Choppin et al., 1989) (Fig. 13). The resolution of the seismic data on seismic transect 2 makes it difficult to continue the fault interpretation into the basement

Figure 13. A. Uninterpreted seismic data from seismic transect 2 crossing the central part of the Espino rift characterized by the thick, syn-rift sedimentary fill observed along the rift. Seismic interpretation is modified from Salazar (2006). Well ties shown are summarized in Figure 5. **B**. Interpreted seismic data from seismic transect 2. In this area, the Espino rift is a full graben with greater vertical throw on the listric, normal fault forming its southeastern boundary. Two anticlinal structures within the rift are either post-rift inversion structures of latest Jurassic age or Jurassic, syn-rift, rollover structures formed by motion along the listric normal faults (Salazar, 2006). Major bounding normal faults of the Espino rift (Ruiz-Saban and Anibal) show listric profiles and were previously mapped by Salazar (2006). Syn-rift thickening along these normal faults is more pronounced for the Jurassic section rather than the Cambrian-Ordovician section, although the latter section is only partially imaged on the line. **C.** Map of the Espino rift in green showing location of seismic transect 2 (red line) across its central part of the rift

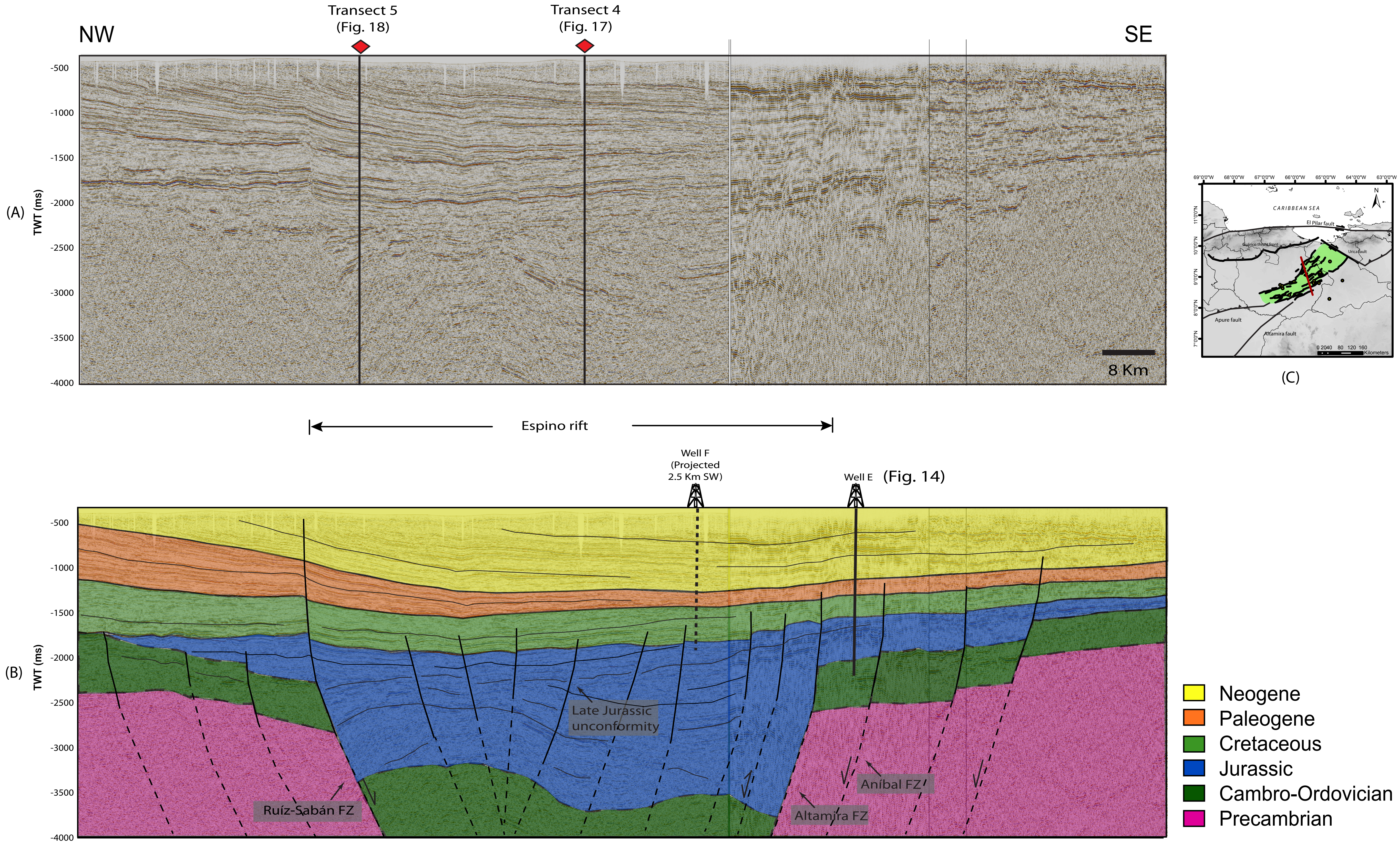

Transect 5
(Fig. 18)
Transect 4
(Fig. 17)
NW
SE
(A)
TWT (ms)
-500
-1000
-1500
-2000
-2500
-3000
-3500
-4000
8 Km
(C)
CARIBBEAN SEA
El Pilar fault
Apure fault
Altamira fault
Espino rift
Well F
(Projected
2.5 Km SW)
Well E
(Fig. 14)
(B)
TWT (ms)
Late Jurassic
unconformity
Ruíz-Sabán FZ
Altamira FZ
Aníbal FZ
Neogene
Paleogene
Cretaceous
Jurassic
Cambro-Ordovician
Precambrian

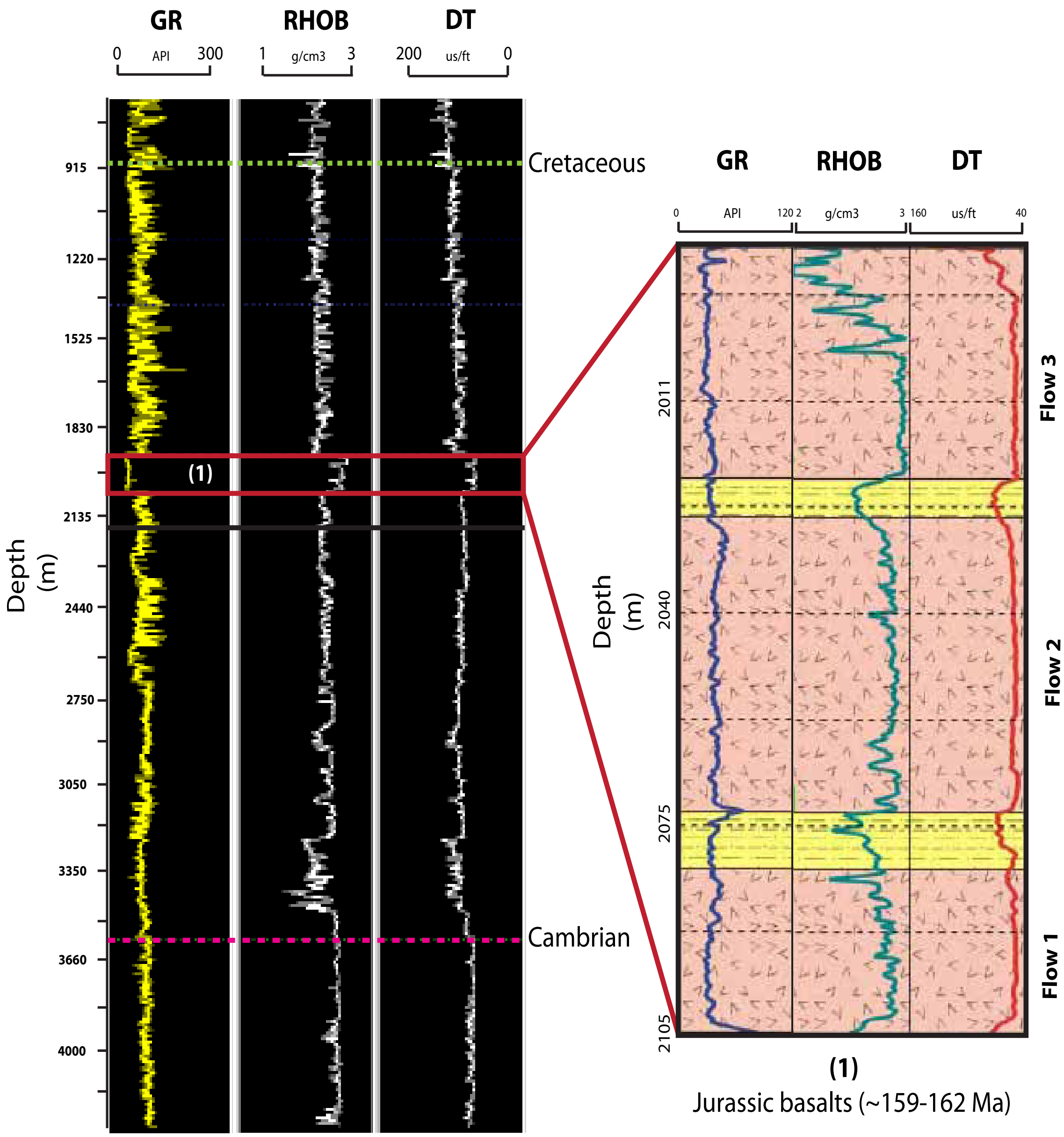

Figure 14. Well logs (Gamma ray (GR), density and sonic) showing the presence of Jurassic basalt flows within sedimentary rocks of the Ipire formation (logs are modified from Salazar, 2006). Zoomed section shows three basalt flows within a sandstone section (modified from Uzcátegui, 2002 and Salazar, 2006)

The Jurassic syn-rift section along the Tinajones fault indicates that the fault originated as a normal growth fault during the Jurassic rift event (Fig. 13). Alternatively, Salazar (2006) and Arminio et al. (2001) proposed that the folds in this area of the Espino rift were generated as roll-over structures on listric normal faults during late Jurassic time. Similarly to Transect 1 (Fig. 12), the uppermost Late Jurassic unconformity may have formed as a breakup unconformity separating Jurassic, syn-rift sections tilted during the rift phase from the overlying, flat-lying Cretaceous rocks that were deposited after normal faulting had ended.

Figure 14 shows Well E (NZZ-88X well in Salazar, 2006), which is one of the few exploration wells that has penetrated and documented Cambrian shale of the Hato Viejo and Carrizal Formations along with Jurassic basalts within the overlying Ipire formation (Fig. 14). These Jurassic basalts, known locally in the Espino rift as the Altamira basalts, are the only direct, evidence of Jurassic volcanism in the Espino rift that has been found to date.

Motiscka (1985) suggests that the Jurassic basalts formed as flows rather than as sills or dikes because: 1) there is no visible, thermal alteration of the overlying sediments adjacent to the basalt layer in the core; and 2) the finely crystalline nature of the basalt from the core suggested it cooled quickly as a flow.

The Ipire formation (Fig. 3) with interbedded basalts is illustrated using its well log in Figure 14. Three basaltic flows are interbedded with late Jurassic shale and siltstone (Uzcátegui, 2002). Radiometric dating shows that the age of one of the basaltic flows is about 162 Ma, or late Jurassic (Motiscka, 1985). These basalts are found beneath a limited area of the central part of the Espino rift bounded by the Anibal and Altamira faults (Salazar, 2006). In general, the Ipire formation is composed sandstone and shale containing local presence of Early to Late Jurassic spores and pollen (Corollina, Callialasporites) (Moticska, 1985).

2.5.3 Seismic transect 3 orthogonal to the Northern Espino rift

Seismic transect 3 extends 150 km at right angles to the northeastern section of the Espino rift (Fig. 15). The Guama-Sabán normal fault represents the northeastern edge of the Espino rift and it is characterized by the presence of the deeper Paleozoic, Guama depocenter located to the west of the Guama-Saban fault (Salazar, 2006). This area shows thicker, Jurassic sedimentary section faulted against the Guama-Sabán fault with sedimentary rocks thinning to the east. Both bounding faults cut into the basement and were active from Cambro-Ordovician to Neogene.

Figure 15. A. Uninterpreted seismic data from seismic transect 3 crossing the northern part of the Espino rift with an intermediate thickness, syn-rift sedimentary fill. Seismic interpretation is modified from Salazar (2006). Well ties shown are summarized in Figure 5. **B.** Interpreted seismic data from seismic transect 3. In this area, the Espino rift exhibits a full graben morphology in cross section with roughly equal amounts of vertical throw on both listric faults (Guama-Saban and Anibal faults, as previously mapped by Salazar, 2006). The Tinajones transfer fault described by Salazar (2006) is a high-angle, right lateral strike-slip fault that cuts obliquely across the basin in this area and may account for formation of the large syncline seen on this line

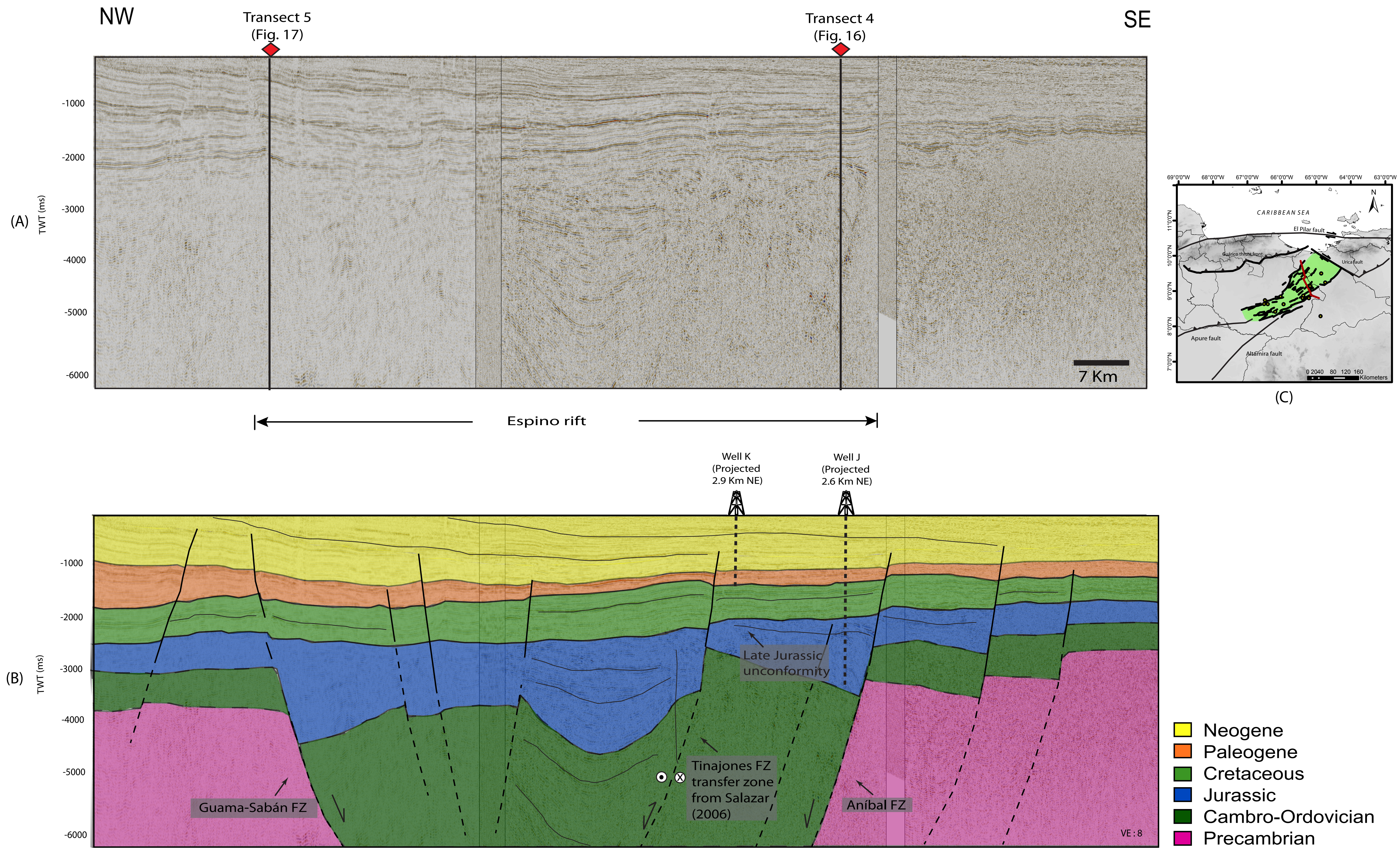
NW
SE
Transect 5
(Fig. 17)
Transect 4
(Fig. 16)
(A)
TWT (ms)
-1000
-2000
-3000
-4000
-5000
-6000
7 Km
CARIBBEAN SEA
El Pilar fault
Apure fault
Altamira fault
Kilometers
(C)
Espino rift
Well K
(Projected
2.9 Km NE)
Well J
(Projected
2.6 Km NE)
(B)
Late Jurassic
unconformity
Tinajones FZ
transfer zone
from Salazar
(2006)
Guama-Sabán FZ
Aníbal FZ
VE : 8
Neogene
Paleogene
Cretaceous
Jurassic
Cambro-Ordovician
Precambrian

The northern part of the rift shows evidence for late Cenozoic fault inversions especially in the area of the Tinajones transfer fault (Salazar, 2006) (Fig. 13). The uppermost, Late Jurassic unconformity is related to either the breakup unconformity separating Jurassic rifted rocks below from un-rifted, passive margin rocks above, or a latest Jurassic, convergent deformation event (Fig. 15).

2.5.3 Seismic transects 4 and 5 parallel to long axis of the Espino rift

Seismic transect 4 extends about 190 km parallel to the bounding normal faults of the Espino rift (Fig. 16). This line shows the rift basement becoming deeper in a northeastward direction where the Espino rift eventually becomes deeply buried by the Cenozoic sedimentation along the transpressive Urica fault (Munro and Smith, 1984). Shallow basement is visible to the southwest along the Altamira high but becomes too deep for seismic resolution in the northwestward direction (Fig. 16). Broad folds are visible in the Paleozoic and Jurassic section and they may be formed as roll-over structures as proposed by Salazar (2006) or by a terminal late Jurassic, convergent event.

Seismic transect 5 extends 210 km parallel to the bounding faults of the Espino rift (Fig. 17). This line is located near the northwestern end of the Espino rift and shows a shallow basement to the southwest, that could be related to the Cambrian rifting and a deeply buried basement to the northeast (not visible in seismic) that may represent the effects of Jurassic rifting superimposed on the earlier Paleozoic rifting event.

Figure 16. A. Uninterpreted seismic data from seismic transect 4 along the long axis of the Espino rift showing the thickening towards the northeast of the syn-rift fill and overlying Cenozoic foreland basin section. Well ties shown are summarized in Figure 5. **B.** Interpreted seismic data from seismic transect 4. Syn-rift thickening along these normal faults is more pronounced for the Cambrian-Ordovician section rather than for the Jurassic section. **C.** Map of the Espino rift in green showing location of seismic transect 4 (red line) running parallel to the rift axis

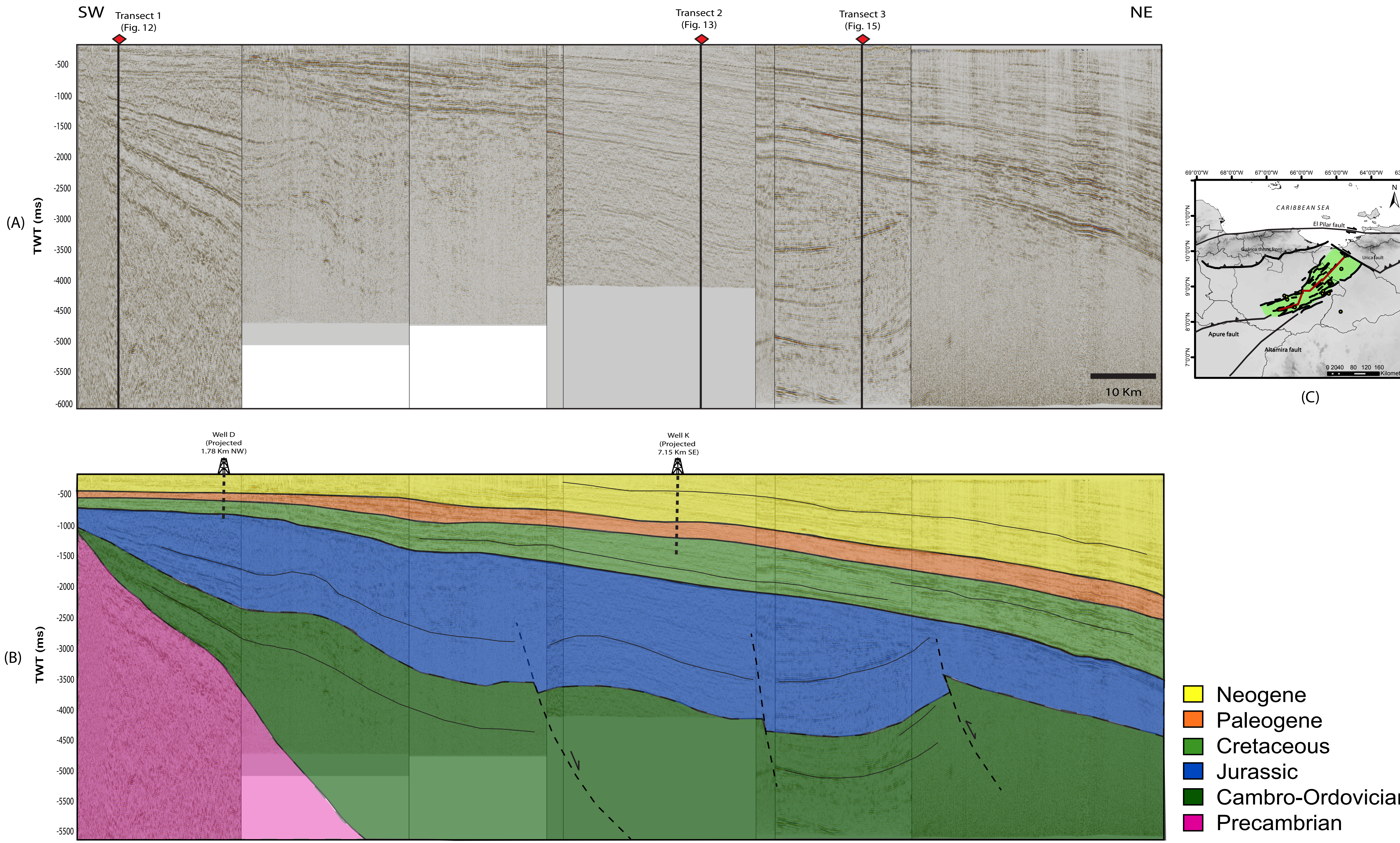

SW
NE
Transect 1
(Fig. 12)
Transect 2
(Fig. 13)
Transect 3
(Fig. 15)
(A)
TWT (ms)
10 Km
(B)
Well D
(Projected
1.78 Km NW)
Well K
(Projected
7.15 Km SE)
(C)
CARIBBEAN SEA
El Pilar fault
Apure fault
Altamira fault
Neogene
Paleogene
Cretaceous
Jurassic
Cambro-Ordovician
Precambrian

Figure 17. A. Uninterpreted seismic data from seismic transect 5 along the long axis of the Espino rift showing the thickening of the rift fill and overlying Cenozoic foreland basin section in the northeast direction. Well ties shown are summarized in Figure 5. **B.** Interpreted seismic data from seismic transect 5. Syn-rift thickening along these normal faults is more pronounced for the Cambrian-Ordovician section rather than the Jurassic section. **C**. Map of the Espino rift in green showing location of seismic transect 4 (red line) running along the rift axis

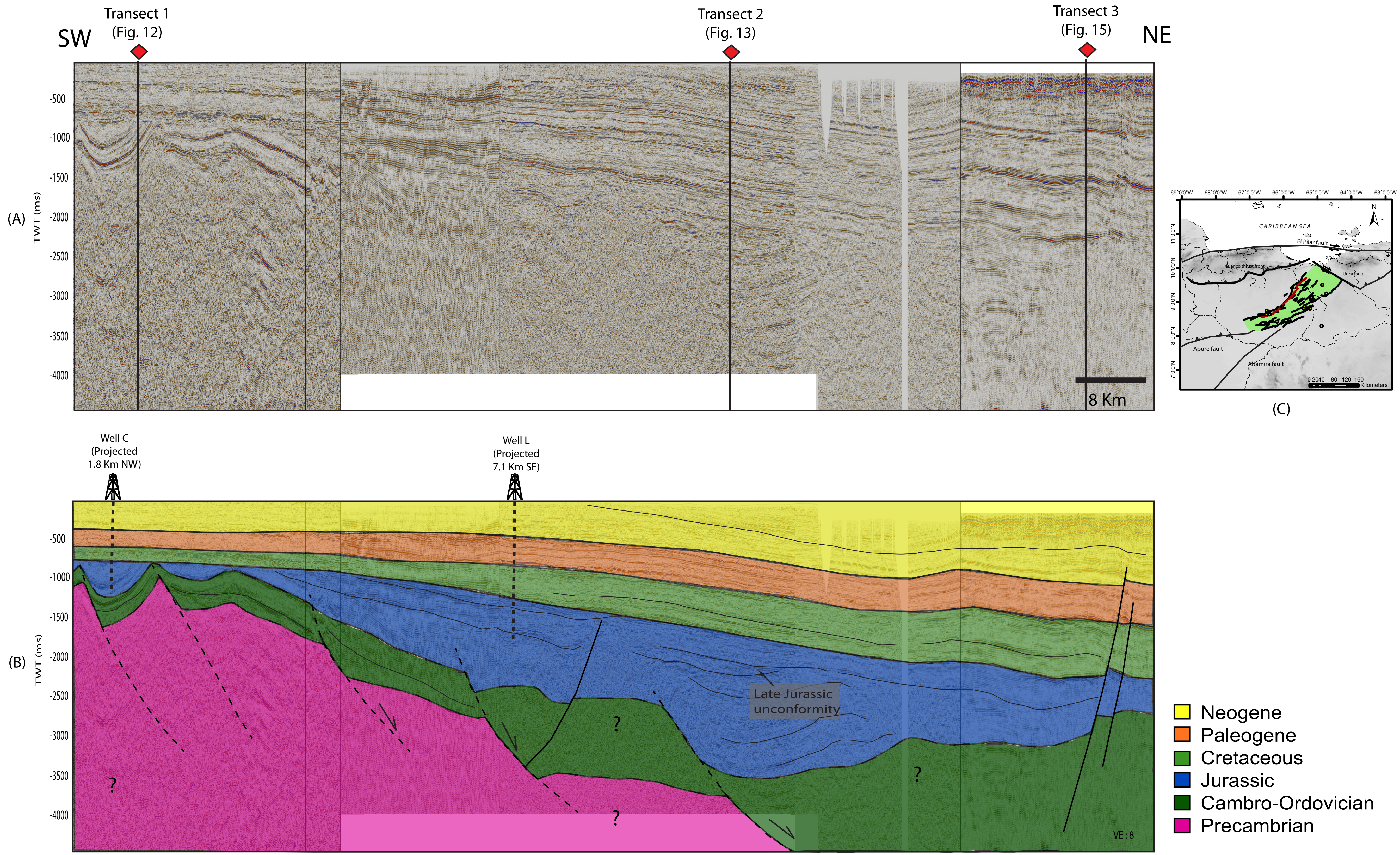
SW
NE
Transect 1
(Fig. 12)
Transect 2
(Fig. 13)
Transect 3
(Fig. 15)
(A)
TWT (ms)
-500
-1000
-1500
-2000
-2500
-3000
-3500
-4000
8 Km
(C)
CARIBBEAN SEA
El Pilar fault
Urica fault
Apure fault
Altamira fault
Kilometers
Well C
(Projected
1.8 Km NW)
Well L
(Projected
7.1 Km SE)
(B)
TWT (ms)
-500
-1000
-1500
-2000
-2500
-3000
-3500
-4000
Late Jurassic
unconformity
?
VE : 8
Neogene
Paleogene
Cretaceous
Jurassic
Cambro-Ordovician
Precambrian

2.6 DISCUSSION

2.6.1 Comparison of previous models for the crustal structure of the Espino rift with my proposed model from this thesis

Previously proposed models for the crustal structure of the Espino rift are seen in Figure 18 and include models by: Laske et al. (2013), Crust 1.0 (Fig. 18A and 18B), Bezada et al. (2010) (Fig. 18C and 18D) and my model from this thesis study based on gravity modeling integrated with regional seismic reflection lines (Fig. 18E and 18F).

Laske et al. (2013) refined the previous model Crust 2.0 by Bassin et al. (2000) and the model proposed by Mooney et al. (1998). The Moho depth in Laske et al. (2013) (Fig. 18B) is based on 1-degree averages of an updated database of crustal thickness from active source seismic studies and from receiver function studies (Laske et al., 2013). Laske and Masters (1997) generated a global onshore sedimentary thickness model which was subtracted from the topo terrain model (NGDC) to obtain depth to basement (Fig. 18A).

Bezada et al. (2010) used the refraction station information obtained in the BOLIVAR-GEODINOS project (Schmitz et al., 2008) and earthquake information to estimate depth to basement (Fig. 17C) and depth to Moho (Fig. 18D) using interpolation methods from the different observations.

The basement depth model for the Espino rift proposed by Laske et al. (2013) (Fig. 18A) ranges from ~700 m to the southwest and ~2500 m to the northeast, supporting shallowing of the Espino rift basement to the southwest and deepening to the northeast.

Their Moho depth model (Fig. 18B) shows no thinning of the crust beneath the Espino rift, with a thickness range of 40-45 Km beneath the Espino rift.

Bezada et al. (2010) proposed a basement depth model ranging between 1000 m in the southern Espino rift and 5000 m in the northern Espino rift (Fig. 18C). Their Moho depth model reveals an area of the crust related to the Cambrian and Jurassic rifting events with depths of ~25-30 km within the Espino rift, and +30 km in the rift flanks (Fig.18D). The lack of refraction information within the Espino rift and the low resolution from the grid size could explain on the differences between basement depths in Bezada et al. (2010) maps and those in this thesis.

Previous models proposed (Bezada et al. (2010) (Fig. 18C, 18D), Laske et al. (2013) (Fig.18B), Laske and Masters (1997) and (NGDC, 2015) (Fig. 18A) all show differences with my proposed model (Fig. 17E and 17F). The main differences in basement depth compared to the models of this study in the Espino rift are +10.5 km (Laske and Masters (1997); (NGDC)) and +2.5 km (Bezada et al., 2010); the differences in Moho depth are +5 km (Bezada et al., 2010). These differences could be associated to the non-uniqueness in the gravity and magnetic modeling, over-interpolation using mainly not located within or adjacent to the Espino rift.

Figure 18. Interpretations by previous workers using gravity, magnetic and refraction data to estimate the top of crystalline basement in the region of the Espino rift compared to the results in this thesis: **Top of crystalline basement: A)** Laske et al. (2010), **C)** Bezada et al. (2010); and NGDC) this thesis; and **Depth to Moho: B)** Laske et al., (2010), **D)** Bezada et al. (2010), compared to the interpretation of this thesis shown in **E)** and **F),** respectively

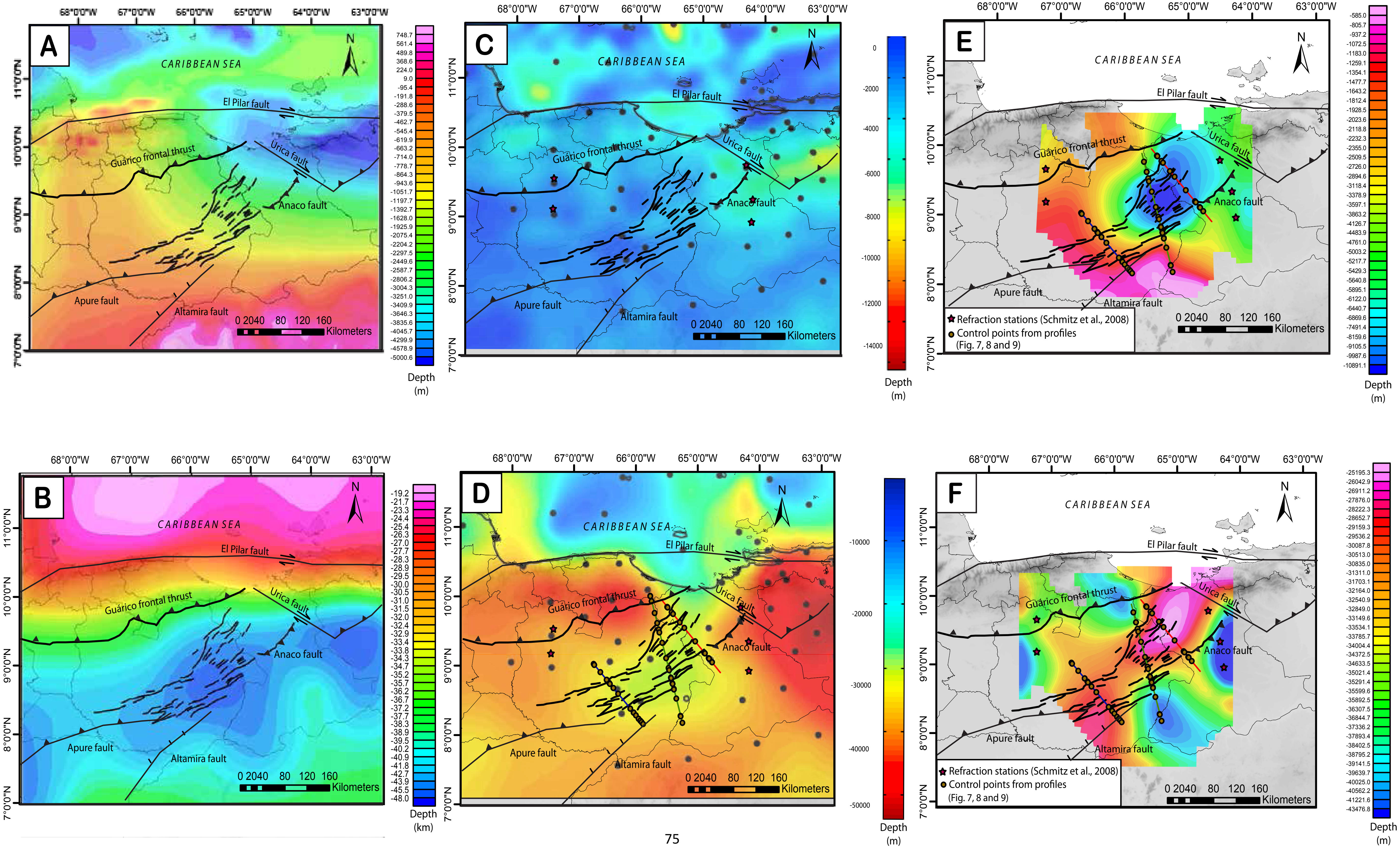
A
B
C
D
E
F
CARIBBEAN SEA
N
El Pilar fault
Guárico frontal thrust
Urica fault
Anaco fault
Apure fault
Altamira fault
0 20 40 80 120 160 Kilometers
68°0'0"W
67°0'0"W
66°0'0"W
65°0'0"W
64°0'0"W
63°0'0"W
11°0'0"N
10°0'0"N
9°0'0"N
8°0'0"N
7°0'0"N
Refraction stations (Schmitz et al., 2008)
Control points from profiles (Fig. 7, 8 and 9)
Depth (m)
Depth (km)

2.6.2 Total magnetic intensity after upward continuation (10 km) showing 25 km of right-lateral strike slip displacement in the Anaco area, northwestern Guayana Shield

The total magnetic intensity map after upward continuation (10 km) revealed a possible, right-lateral, strike-slip fault offsetting three, linear, magnetic highs and lows in the northwestern part of the Guayana shield (Fig. 19A). These linear anomalies are 60-80 km wide and can be traced over along-strike distances of 200-280 km in a northeasterly direction and are numbered 1-3 on Figure 19A, B. The proposed strike-slip fault strikes to the northwest and offsets the anomalies in a right-lateral sense by 25 km. In Figure 19B, I have restored the anomalies and apparent fault offset to show the close match between the trends and widths of the three magnetic highs and their adjacent magnetic lows. The northwestern end of the proposed fault intersects the southwestern Espino rift in the area where the Paleozoic and Jurassic syn-rift fill is thinnest. In the pre-fault reconstruction shown in Figure 19B, the single and continuous magnetic high formed by the Espino rift is offset by about 25 km in a left-lateral sense (Fig. 19B).

There are three possible models for the formation of the proposed fault: 1) the fault is Precambrian in age and predates both the Paleozoic and Jurassic rift phases in the Espino rift; 2) the fault formed as a transfer fault during one or both of the rift phases: the right-lateral offset would explain why the central and northern part of the Espino rift is wider and deeper than the part of the rift southwest of the fault; and 3) the fault formed as a result of oblique plate deformation between the Caribbean and South American plates in the Cenozoic; the northern and central parts of the Espino rift would have been transported

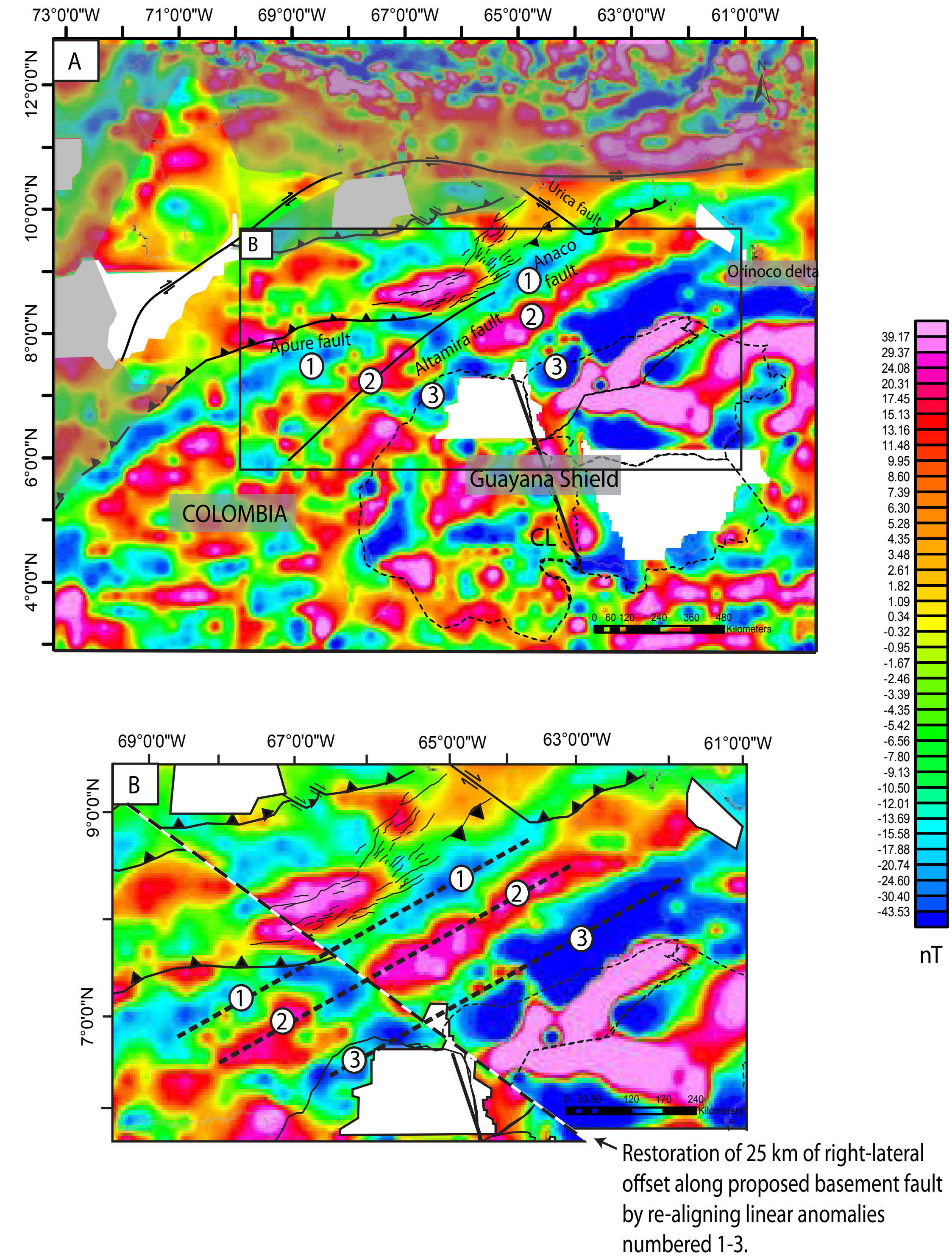

Figure 19. A. Map of total magnetic intensity after upward continuation of 10 km. The anomalies labeled 1, 2 and 3 show a right-lateral offset of 25 km. B. Zoomed section showing the anomalies 1, 2 and 3 restored along a prposedright-lateral, strike slip fault shown as the dashed line.

further to the southeast in a right-lateral sense as a result of oblique Caribbean convergence..

2.6.3. Comparison of structure and stratigraphy of the Espino syn-rift sedimentary and volcanic fill proposed in this study with those of previous studies

As shown in the fence diagram (Fig. 20), the Espino rift exhibits a typical rift structure including listric, normal faults (Morley et al. 1990). The rift shows its shallower section to the southwest becoming deeper to the northeast. Gravity data shows thickness of Cambrian-Ordovician sections between 3800 and 4000 m interpreted from gravity transects B and C (Fig. 8 and 9). A combination of a depth estimate from velocity information compiled in Figure 5 with two-way travel time information in transects 2 and 3 (Figs. 13, 15) provide a minimum thickness consistent with the thicknesses inferred from gravity transects.

The Paleozoic and Jurassic syn-rift fills appear conformable throughout the rift although a major unconformity is necessary to separate the Cambro-Ordovician section from the overlying Jurassic section or period of non-deposition (Figs. 12, 13, 15, 16 and 20). Broad folds and inverted normal faults characterize both the Paleozoic and Jurassic syn-rift sections (Figs. 13, 15 and 20). Previous workers have proposed various models for deformation of the Espino group that include:

Figure 20. Fence diagram of the Espino rift combining seismic transects 1, 2, 3 and 4 and wells A, B, C, D, E, L, K and H that are summarized in Figure 5. The along-strike variation in the syn-rift, sedimentary thickness of the rift varies from thickest in the central and northern parts of the rift and thinnest in the southwestern part of the rift

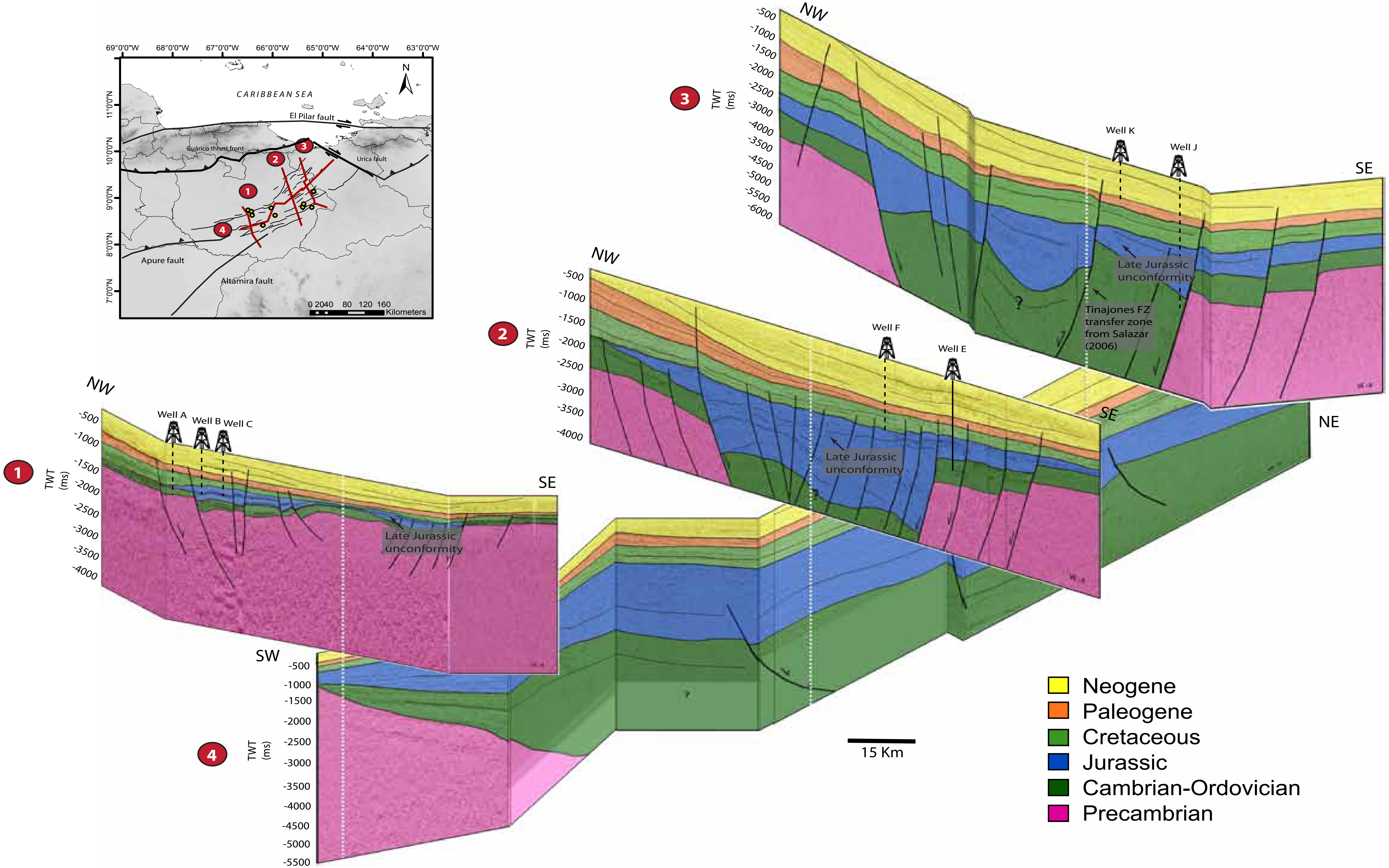
CARIBBEAN SEA
El Pilar fault
Guárico thrust front
Urica fault
Apure fault
Altamira fault
Kilometers
NW
SE
SW
NE
TWT (ms)
Well A
Well B
Well C
Well E
Well F
Well K
Well J
Late Jurassic unconformity
Tinajones FZ transfer zone from Salazar (2006)
15 Km
Neogene
Paleogene
Cretaceous
Jurassic
Cambrian-Ordovician
Precambrian

1) Transect 2 and 3 show that there is no apparent angularity between the Paleozoic and Jurassic sections to support the existence of the proposed Paleozoic convergence event proposed by Ross and Scotese (1988) (Fig. 13 and 15).

2) Salazar (2006) proposed that syn-rift normal faults produced rollover folds and localized unconformities. This model would predict unconformities throughout the section of both the Paleozoic and Jurassic syn-rift sections. On transects 2, 3 and 4 (Fig. 13, 15 and 16) I observe that major unconformities are present within near the upper part of the Jurassic, syn-rift section rather than at all levels within the rift as might be expected if the unconformity formed as roll-over structure during the rifting phase.

3) Salazar (2006) also proposed that the Tinajones transfer fault was active during the Jurassic opening of the Espino rift and produced transpressional deformation in this northern part of the rift that included the inversion nearby, pre-existing normal faults. Other transfer faults active during both rifting events might be present including the right-lateral, strike-slip fault identified on Figure 19. Deformation along transfer faults would not predict widespread convergence in the rift outside the areas of the transfer faults.

4) Another possible deformation mechanism for the Espino rift is a period of shortening associated with the angular unconformities present at the top of the Jurassic rift section as shown in Figures 13 and 15. These unconformities document the timing of large folds that formed at this time and were beveled off and overlain by less deformed, syn-rift rocks (Fig. 20). These unconformities are ~100 m below the "breakup unconformity" present at the top of the Jurassic, syn-rift section and beneath the overlying and undeformed Cretaceous, passive margin section (Fig. 20). The mechanism for a short-lived Jurassic compressional event is not known but might be similar to the large-scale shortening that

affected Jurassic syn-rift rocks of the Demerara Rise, 620 km to the east of the Espino rift (Reuber et al., 2016).

The final mechanism for possible convergent deformation in the Espino rift is Cenozoic shortening related to the oblique collision between the Caribbean and South American plates. This mechanism may have led to localized inversion of normal faults including the Anaco fault in the northern Espino rift and the presence of inverted normal faults but no widespread folding or unconformities is observed on the seismic transects.

2.6.4. Relation and timing of the Paleozoic and Jurassic Espino rifts to larger-scale plate tectonic events

The northeast trend of the Espino rift is sub-parallel to other Cambrian rifts int the Appalachian Mountains of the eastern USA and that is its likely Paleozoic conjugate margin (Fig. 1). The Triassic and Jurassic opening between North and South America was in the same direction as the Cambrian rifting event and reactivated the older Cambrian rift in northern South America (Fig. 1).

The Central Atlantic magmatic province (CAMP) is a large igneous province of 200 Ma age mainly composed of basalts in flows and intrusive bodies formed in the Late Triassic-Early Jurassic present in the North and South America, Europe and northwest Africa (Blackburn et al., 2013). The South American extension of this province is relatively close to the Espino rift (Fig. 1), however, the Jurassic basalts found in Well E in the central-north section of the rift are of much younger age 162 Ma (Late Jurassic) and limited to the Espino rift.

2.6.5 Burial history

The subsidence plot for well E (Fig. 21) located on the eastern edge of the Espino rift shows the main tectonic phases of the Espino rift. Well E does not provide a representative thickness for the syn-rifting, sedimentary section because Well E does not penetrate the thickest, syn-rift units along the central axis of the rift. However, well E does penetrate most of the Paleozoic to Cenozoic stratigraphic units present in the Espino rift (Fig. 14)

Cambro-Ordovician rifting controlled the deposition of +1500 m of marine sediments of Carrizal and Hato Viejo formations from approximately 529 Ma to 440 Ma (Late Cambrian). Erosion occurred approximately 430 Ma to 252 Ma (Middle Silurian-Late Permian) and likely marks the orogenic highlands generated by the collison that formed the Pangean supercontinent. Pangea began to break up about 175 Ma (late Jurassic) with the formation of the Central and South Atlantic Oceans. During this rifting, approximately 1640 m of continental sediments of the Ipire formation of Late Jurassic age were deposited, along with 25-40 m basalt flows of Late Jurassic age (Fig. 14). By the end of rifting in the latest Jurassic, a passive margin setting and the generation of the proto-Caribbean Sea (Fig. 1) formed on the southern flank of the Caribbean Sea with the the deposition of the continental sediments of Canoa and Tigre Formations. The collision between the Caribbean and South American plates generated the Eastern Venezuelan foreland basin with deposition of the shallow marine sediments of the Roblecito, Mercure, Oficina, and lagoonal sediments of the Freites Formation.

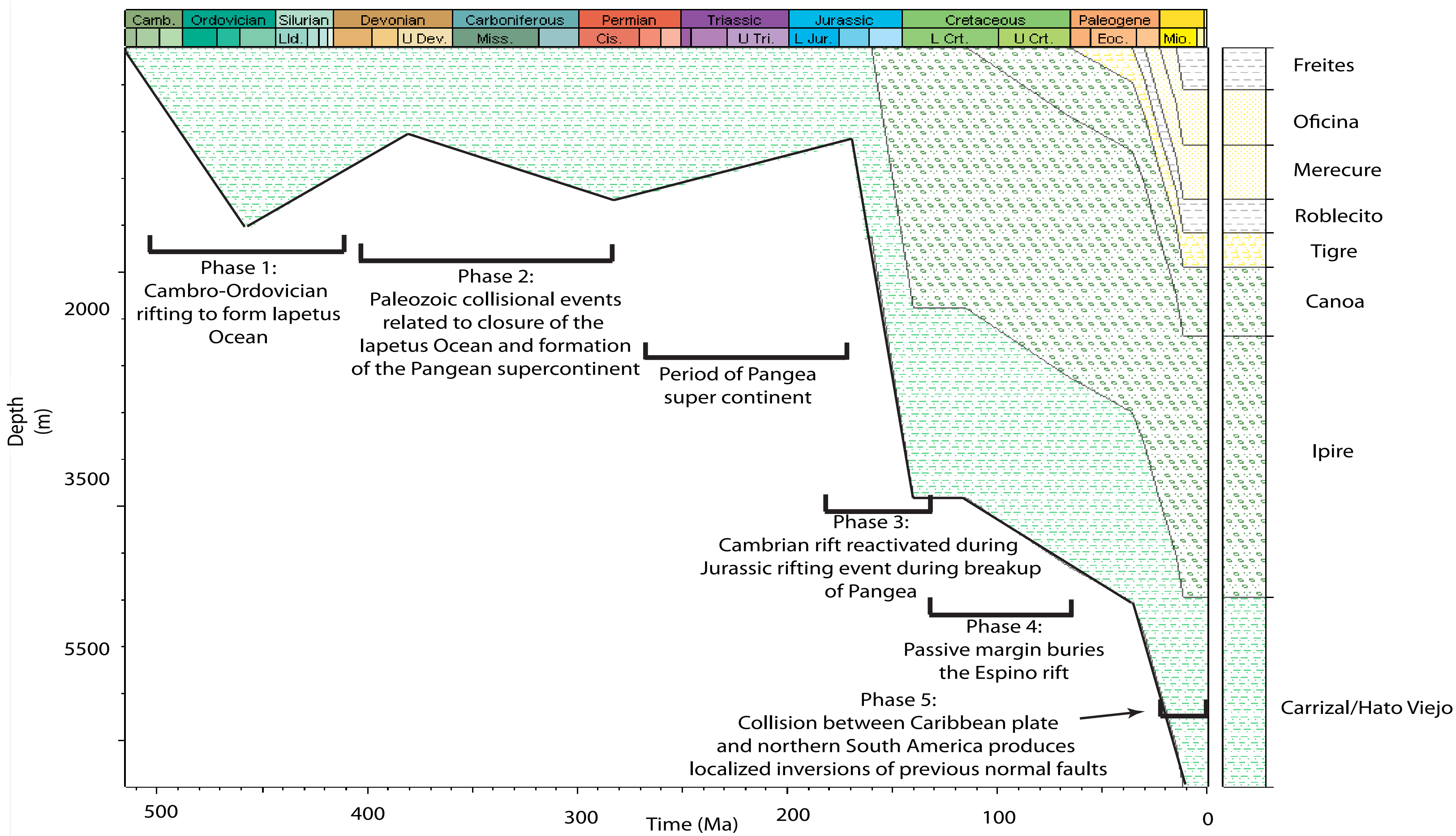

Figure 21. Burial history derived from well E in the Espino rift (located on Figure 14) interpreted as five major tectonic phases: Phase 1 = Cambro-Ordovician rifting; Phase 2 = uplift and erosion event related to late Paleozoic collision of North and South America; Phase 3 = late Jurassic rifting with volcanism along same trend as previous Cambrian-Ordovician rift; Phase 4 = Cretaceous passive margin; and Phase 5 = oblique collision between the Caribbean plate and northern South America results in burial beneath the Eastern Venezuelan foreland basin

2.7. CONCLUSIONS AND RECOMMENDATIONS

1. The Espino rift is a major continental rift located on continental crust of northern South America. The rift is buried beneath the Guárico sub-basin of the Eastern Venezuelan foreland basin. The Espino rift which was affected by: 1) Cambro-Ordovician rifting; 2) Late Paleozoic collision event between North and South America to form the supercontinent Pangea; 3) late Jurassic rifting between North and South America that accompanied the breakup of the supercontinent Pangea; and 4) Cretaceous passive margin subsidence following rifting; Cenozoic to present transpression between the Caribbean plate and northern South America. The Espino rift is located near or along the Caledonian suture zone separating Precambrian rocks of the Guayana shield from a Paleozoic orogenic belt along its northern and northwestern margin.

2. Gravity and magnetic anomaly interpretations using filters and enhancements showed the different signals from the region of the Espino rift that can be related to geological features, faults, tectonic contacts, and igneous-metamorphic provinces.

3. Gravity modeling along three transects at right angles to the long axis of the Espino rift shows that the syn-rift fill is thinner to the southwest (300m) and deepens to the northeast (1200 m). This southwest to northeast sedimentary thickening reflects a decrease in crustal thickness from southwest to northeast.

4. Depth to basement and depth to Moho maps showed consistency with the result of refraction measurements and previous gravity modeling. Modeling of gravity and data

in this thesis showed a deeper top crystalline basement (~10 km) and shallower top Moho (~25 km) than in interpretations by previous workers.

5. Seismic reflection interpretation showed structures related to rifts previously proposed by Salazar (2006) including the Tinajones transfer fault that may have formed during the Jurassic rifting phase and led to localized inversion of nearby normal faults. The break-up unconformities described by Nottvedt et al. (1995) in the North Sea is resent in the Espino rift, separating rifted rocks from overlying passive margin rocks.. Inverted structures in the rift, such as the Altamira High, show evidence for compressional events within the rift that range in age from at least Jurassic to Cenozoic.

6. Possible future studies of the Espino rift based on the results from this thesis include: 1) acquisition of new, 2D seismic reflection surveys with wider offset to improve mapping of the Cambro-Ordovician, syn-rift fill; and 2) acquisition of new refraction within the Espino rift to better constrain the depth to basement and to the Moho beneath the rift.

2.8 REFERENCES

Arminio, J. F., Yoris, F., Quijada, C., Lugo, J. M., Shaw, D., Keegan, J. B., and Marshall, J. E., 2011, Evidence for Precambrian stratigraphy in graben basins below the Eastern Llanos Foreland, Colombia: AAPG International Conference and Exhibition, Cartagena, Colombia. Search and Discovery Article #50874.

Audemard, F. and Serrano, I., 2001, Future petroliferous provinces of Venezuela, Downey M., J. Threet and W. Morgan. (eds.): Petroleum provinces of the twenty-first century, AAPG Memoir, v. 74, p. 353 – 372.

Bartok, P., 1993, Prebreakup geology of the Gulf of Mexico- Caribbean: Its relation to Triassic and Jurassic rift systems of the region: Tectonics, v. 12, p. 441-459.

Bartok, P., 2003, The peripheral bulge of the Interior Range of the Eastern Venezuela basin and its impact on oil accumulations, Bartolini, R. T. Buffler, and J. Blickwede, eds.: The Circum-Gulf of Mexico and the Caribbean: Hydrocarbon habitats basin formation, and plate tectonics: AAPG Memoir 79, p. 925-936.

Barrios, Y. A., Baptista, N., and Gonzales, G., 2011, New exploration traps in the Espino Graben, Eastern Venezuela Basin: AAPG Annual Convention and Exhibition, Houston, Texas, USA, Search and Discovery Article #10333.

Bellizzia G. A, 1972, Is the Entire Caribbean Mountain Belt of Northern Venezuela Allochthonous?: Studies in earth and space sciences, Memoir of the Geological Society of America, v. 132, p. 363-368.

Bellizzia, C. M., and Bellizzia, A., 1956, Imataca Series: Stratigraphic lexicon of Venezuela, Ministerio de Minas e Hidrocarburos, Special Publication, v. 01, p. 254-256.

Blackburn, T. J., Olsen, P. E., Bowring, S. A., McLean, N. M., Kent, D. V., Puffer, J., and Et-Touhami, M., 2013, Zircon U-Pb geochronology links the end-Triassic extinction with the Central Atlantic Magmatic Province: Science, v. 340(6135), p. 941-945.

Blakely, R. J., 1996, Potential theory in gravity and magnetic applications. Cambridge University Press, 445 p.

Blanco, J., Mann, P., Bartok, P., 2013, Subsurface structure, stratigraphy and hydrocarbons of the Falcon Basin: An inverted, hydrocarbon-bearing rift basin in western Venezuela: AAPG ICE Conference, Cartagena, Colombia.

Briceño, H.; Tapia, J. and Estanga, J., 1989, Formacion Ichun, volcanimos acido de Grupo Roraima: VII Cong. Geol. Venez, Barquisimeto, Estado Lara, v. 1, p. 57-82.

Choppin H., Gonzalez A., Rodriguez, H., Roux, E. and Uzcategui M., 1989, Síntesis Estratigráfica y Tectónica de Anzoategui y Guárico Este (SETAGE): Tomo II. Geofísica. Informe Interno Corpoven, 200 p.

Christenson, G. L., Mann, P., Escalona, A., Aitken, T. J., 2008, Crustal structure of the Caribbean-northeastern South America arc-continent collision zone: Journal of Geophysical Research, v. 113 (B12).

Clark, S.A., Sobiesiak, M., Zelt, C.A., Magnani, M., Levander, A., 2008b, Characterizing the Caribbean-South American plate boundary at 64 degrees W using wide angle seismic data: Journal of Geophysical Research, v. 113(B7).

Dalla Salda, L., Cingolani, C., & Varela, R., 1992, Early Paleozoic orogenic belt of the Andes in southwestern South America: Result of Laurentia-Gondwana collision?: Geology, v. 20(7), p. 617-620.

Di Croce, J., 1996, Eastern Venezuela Basin: Sequence stratigraphy and structural evolution: Unpublished PhD dissertation, Rice University, 225 p.

Durán, E., 2007, Inversión gravimétrica 3D en el Graben de Espino: Trabajo de Grado, Universidad Simón Bolívar, Caracas, Venezuela, Maestría en Ciencias de la Tierra, 127 p.

Escalona, A., and Mann, P., 2011, Tectonics, basin subsidence mechanisms, and paleogeography of the Caribbean-South American plate boundary zone: Marine and Petroleum Geology, v. 28(1), p. 8-39.

Feo-Codecido, G., Smith, F. D., Aboud, N., & de Di Giacomo, E., 1984, Basement and Paleozoic rocks of the Venezuelan Llanos basins: Geological Society of America Memoir, v. 162, p. 175-188.

Figueroa, L., Díaz Martínez, R., Oña Alvarez, R., Rodríguez Vega, A., Boggio Marcano, W. and Pérez Díaz, R., 2011, Caracterización petrológica y geofísica del complejo de Imataca en el sector La Quina. Estado Bolívar, Venezuela: IX Congreso Cubano de Geología, p. 11.

Fiorillo, G., Ortega, J., Ramos C., Gowen, K. y Bass, I., 1981, Revisión Geológica-Geofísica de la Faja Petrolífera del Orinoco: Reporte Interno PDVSA, 305 p.

Galavis , J. and Velarde, H., 1967, Geological study and preliminary evaluation of potential reserves of heavy-oil of the Orinoco tar belt, Eastern Venezuelan basin: 7th World Petroleum Congress (Ciudad de México), v. 7, p. 229-234.

García, A., 2009, Mapas de anomalías de gravedad y magnetismo de Venezuela generados a partir de datos satelitales: Trabajo de Grado, Universidad Central de Venezuela, Caracas, Venezuela, 199 p.

Gibson, R. I., and Millegan, P. S., 1998, Geologic applications of gravity and magnetics: case histories: Published jointly by the Society of Exploration Geophysicists and the American Association of Petroleum Geologists, 171 p.

Gonzales de Juana, C., de Arozena, J. M. I., and Cadillat, X. P, 1980, Geología de Venezuela y de sus Cuencas Petrolíferas, v. 2, 1034 p.

González, W., 2009, Interpretación del basamento precretácico en las cuencas Barinas-Apure y Oriental de Venezuela: Trabajo de grado, Maestría, Universidad Simón Bolívar, Caracas, Venezuela, 198 p.

Guédez, M., 2007, Crustal structure across the Caribbean-South American plate boundary at 70W-Results from seismic refraction and reflection data: Unpublished MS. Thesis, Rice University, 175 p.

Hedberg, H., 1950, Geology of the eastern Venezuela basin (Anzoátegui-Monagas-Sucre-eastern Guárico portion): Geological Society of America Bulletin, v. 61(11), p. 1173-1216.

Hurley, P. M., Fairbairn, H. W., Gaudette, H. E., Mendoza, V., Martin, C. B., and Espejo, A., 1973, Progress report on age dating in the northern Guayana Shield: Proceedings 2nd. Latin-American Geological Conference, v. 55(4), 466 p.

Jácome, M. I., Rondón, K., Schmitz, M., Izarra, C., and Viera, E., 2008, Integrated seismic, flexural and gravimetric modelling of the Coastal Cordillera Thrust Belt and the Guárico Basin, North-Central Region, Venezuela: Tectonophysics, v. 459(1), p. 27-37.

Korol, B., 1965, Estratigrafia de la Serie Pastora en la region Guasipati-El Dorado: Cong. Cent. Col. Ing. Venez. Bol. Geol., Caracas, v. 7(13), p. 3-17.

Laske, G., and Masters, G., 1997, A global digital map of sediment thickness: American Geophysical Union, v. 78(F483), p. 483.

Laske, G., Masters, G., Ma, Z., & Pasyanos, M., 2013, Update on CRUST 1.0 A 1-degree global model of Earth's crust: Geophysics Research. Abstracts, v. 15, p. 2658

Li, Y. and Oldenburg, D. W., 1996, 3D inversion of magnetic data: Geophysics, v. 61, p. 394-408.

Linares, M.F.J., 2013, Generación del mapa del basamento de la cuenca de Falcón, a partir de datos gravimétricos y magnéticos satelitales: Trabajo de grado, Universidad Central De Venezuela, Caracas, Venezuela, 129 p.

Lowrie, W., 2007, Fundamentals of geophysics: Cambridge University Press, 393 p.

MacLeod, I. N., Jones, K., and Dai, T. F., 1993, 3-D analytic signal in the interpretation of total magnetic field data at low magnetic latitudes: Exploration Geophysics, v. 24(3/4), p. 679-688.

Martinez, A. R., 1987, The Orinoco Oil Belt, Venezuela: Journal of Petroleum Geology, v. 10(2), p. 125-134.

Maus, S., Barckhausen, U., Berkenbosch, H., Bournas, N., Brozena, J., Childers, V., and Gaina, C., 2009, EMAG2: A 2–arc min resolution Earth Magnetic Anomaly Grid compiled from satellite, airborne, and marine magnetic measurements: Geochemistry, Geophysics, Geosystems, v. 10(8).

McCandless, G. C., 1965, Reconocimiento geológico de la parte occidental del Estado Bolívar: Boletin Geologico de Venezuela, v. 7(13), p. 19-28.

McClay, K, 2001, Structural geology for petroleum exploration: Londres, Royal Holloway, University of London, 503 p.

Moreno-López, M. C., and A. Escalona, 2014, Precambrian-Pleistocene tectonostratigraphic evolution of the southern Llanos Basin, Colombia: AAPG Bulletin, v. 20, p. 1473-1501.

Morley, C., Nelson, R., Patton T. y Munn, S., 1990, Transfer zones in the East African rift System and their relevance to hydrocarbon exploration in Rifts: AAPG Bulletin, v. 74, p. 1234-1253.

Motiscka, C., 1985, Volcanismo Mesozoico en el subsuelo de la Faja Petrolífera del Orinoco, Estado Guárico, Venezuela: VI Congreso Geológico Venezolano, v. 3, p. 1929-1943.

Muessig, K. W., 1984, Structure and Cenozoic tectonics of the Falcón Basin, Venezuela, and adjacent areas. Bonini, W., Hargraves, R. and Shagam, R. (eds).: The Caribbean-South American plate boundary and regional tectonics, Geological Society of America Memoir, v. 162, p. 217-230.

Munro, S. E., & Smith, F. D., 1984, The Urica fault zone, northeastern Venezuela. Bonini, W., Hargraves, R. and Shagam, R., eds.: Falcón Basin, Venezuela, and adjacent areas. Bonini, W., Hargraves, R. and Shagam, R. (eds.): The Caribbean-South American plate boundary and regional tectonics, Geological Society of America Memoir, v. 162, p. 213-215.

National Geophysical Data Center (NGDC): accessed on September 15th, 2015. <https://www.ngdc.noaa.gov/

Nottvedt, A., Gabrielsen, R. H., and Steel, R. J., 1995, Tectonostratigraphy and sedimentary architecture of rift basins, with reference to the northern North Sea: Marine and Petroleum Geology, v. 12(8), p. 881-901.

Ostos, M., Yoris, F., and Lallemant, H. G. A., 2005, Overview of the southeast Caribbean–South American plate boundary zone: Geological Society of America Special Papers, v. 394, p. 53-89.

Parnaud, F., Gou, Y., Pacual, J. C., Capello, M. A., Truskowski, I., and Passalacqua, H., 1995, Stratigraphic synthesis of western Venezuela. Tankard, A. J., Suarez Soruco, R. and Welsink H. J. (eds.) :Petroleum basins of South America, AAPG memoir, v. 62, p. 681-698.

Pavlis, N. K., S. A. Holmes,S. C. Kenyon, and J. K. Factor, 2008, An Earth gravitational model to degree 2160: EGM2008: Journal of Geophysical Research, v. 117(4), p. 150-165.

PDV Lexico. N. p., 1997: accessed May 26th, 2016. <http://www.pdv.com/lexico/>

Pelechaty, S.M., 1996, Stratigraphic evidence for the Siberia–Laurentia connection and early Cambrian rifting: Geology, v. 24, p. 719–722.

Peters, L. J., 1949, The direct approach to magnetic interpretation and its practical application: Geophysics, v. 14(3), p. 290-320.

Portilla, A., 1993, Interpretación Sísmica del Área de Machete, Faja Petrolífera, Estado Guárico: Tesis de Convalidación. Universidad Central de Venezuela, Caracas, Venezuela, 70 p.

Reid, A. R., 1974, Proposed origin for Guianian diamonds: Geology, v. 2(2), p. 67-68.

Restrepo-Pace, P. A., Ruiz, J., Gehrels, G., & Cosca, M., 1997, Geochronology and Nd isotopic data of Grenville-age rocks in the Colombian Andes: new constraints for Late Proterozoic-Early Paleozoic paleocontinental reconstructions of the Americas: Earth and Planetary Science Letters, v. 150(3), p. 427-441.

Reuber, K., Pindell, J. and Horn, B., 2015, Demerara Rise, offshore Suriname: Magnma-rich segment of the Central Atlantic Ocean, and conjugate to the Bahamas hotspot: Interpretation, v. 4(2), p. T31-T45.

Rios, K., 2002, Estimación de espesores sedimentarios del Mesozoico en el graben de Espino a lo largo de dos transectos regionales en el área de Anaco, estado Anzoátegui: Trabajo de Grado. Universidad Central de Venezuela, Caracas, Venezuela, 132 p.

Roest, W. R., Verhoef, J., and Pilkington, M., 1992, Magnetic interpretation using the 3-D analytic signal: Geophysics, v. 57(1), p. 116-125.

Rosendahl, B., 1987, Architecture of continental rifts with special reference to East Africa.: Annual Review of Earth and Planetary Sciences, v. 86, p. 961-6.

Ross, M. I., and Scotese, C. R., 1988, A hierarchical tectonic model of the Gulf of Mexico and Caribbean region: Tectonophysics, v. 155(1), p. 139-168.

Salazar, M., 2006, Evolución estructural e implicaciones tectónicas del Graben de Espino: Trabajo de Grado. Universidad Simón Bolívar. Caracas, Venezuela, Maestría en Ciencias de la Tierra, 214 p.

Schmitz, M., Avila, J., Bezada, M., Vieira, E., Yánez, M., Levander, A, and BOLIVAR Active Seismic Working Group., 2008, Crustal thickness variations in Venezuela from deep seismic observations: Tectonophysics, v. 459(1), p. 14-26.

Schmitz, M., Chalbaud, D., Castillo, J., & Izarra, C., 2002, The crustal structure of the Guayana Shield, Venezuela, from seismic refraction and gravity data: Tectonophysics, v. 345(1), p. 103-118.

Şengör, A. C., and Natal'in, B. A., 2001, Rifts of the world, Ernest, R., Buchan, K. and Jeoloji Bolumu, (eds.): Mantle plumes; their identification through time, Geological Society of America Special Papers, v. 352, p. 389-482.

Seton, M., Müller, R. D., Zahirovic, S., Gaina, C., Torsvik, T., Shephard, G., and Chandler, M., 2012, Global continental and ocean basin reconstructions since 200Ma: Earth-Science Reviews, v. 113(3), p. 212-270.

Speed, R. C., Sharp, W. D., and Foland, K. A., 1997, Late Paleozoic granitoid gneisses of Northeastern Venezuela and the North America- Gondwana collision Zone: The Journal of Geology, v. 105(4), p. 457-470.

Uzcátegui, D., 2002, Estimación de espesores sedimentarios en el Graben de Espino a lo largo de dos transectos regionales entre Guárico y Anzoátegui, Área Santa María de Ipire: Trabajo de Grado, Departamento de Geofísica, Universidad Central de Venezuela, Caracas, Venezuela, 107 p.

Varela, E., 2004, Estudio sedimentológico de las capas rojas en el area machete, estado Guárico: Trabajo de grado. Universidad Central De Venezuela, Caracas, Venezuela, 217 p.

Vega, A., and de Rojas, I., 1987, Exploration and evaluation of the Zuata area, Orinoco oil belt, Venezuela: Journal of Petroleum Geology, v. 10(2), p. 163-176.

Yoris, F., Ostos, M., and Zamora, L., 1997, Petroleum geology of Venezuela: Venezuela Well Evaluation Conference. Schlumberger Surenco. Houston, p. 1-44.

Williams, H., 1995, Geology of the Appalachian—Caledonian Orogen in Canada and Greenland: Geological Survey of Canada, 952 p.